HHS Public Access

Author manuscript

Cancer Cell. Author manuscript; available in PMC 2017 June 21.

Published in final edited form as:

Cancer Cell. 2017 April 10; 31(4): 563–575.e5. doi:10.1016/j.ccell.2017.03.006.

Inhibition of Hematopoietic Cell Kinase Activity Suppresses Myeloid Cell-Mediated Colon Cancer Progression

Ashleigh R. Poh[1,2], **Christopher G. Love**[2], **Frederick Masson**[1], **Adele Preaudet**[2], **Cary Tsui**[2], **Lachlan Whitehead**[2], **Simon Monard**[2], **Yelena Khakham**[2], **Lotta Burstroem**[2], **Guillaume Lessene**[2,3], **Oliver Sieber**[2,4,5], **Clifford Lowell**[6], **Tracy L. Putoczki**[1,2,7], **Robert J.J. O'Donoghue**[1,2,7,*], and **Matthias Ernst**[1,2,7,8,*]

[1]Olivia Newton-John Cancer Research Institute, La Trobe University School of Cancer Medicine, Heidelberg, VIC 3084, Australia

[2]The Walter and Eliza Hall Institute of Medical Research, Department of Medical Biology, University of Melbourne, Melbourne, VIC 3052, Australia

[3]Department of Pharmacology and Therapeutics, University of Melbourne, Melbourne, VIC 3010, Australia

[4]Department of Colorectal Surgery, Royal Melbourne Hospital, Melbourne, VIC 3050, Australia

[5]School of Biomedical Sciences, Monash University, Clayton, VIC 3800, Australia

[6]Department of Pathology and Laboratory Medicine, University of California, San Francisco, CA 94143, USA

SUMMARY

Aberrant activation of the SRC family kinase hematopoietic cell kinase (HCK) triggers hematological malignancies as a tumor cell-intrinsic oncogene. Here we find that high HCK levels correlate with reduced survival of colorectal cancer patients. Likewise, increased Hck activity in mice promotes the growth of endogenous colonic malignancies and of human colorectal cancer cell xenografts. Furthermore, tumor-associated macrophages of the corresponding tumors show a pronounced alternatively activated endotype, which occurs independently of mature lymphocytes or of Stat6-dependent Th2 cytokine signaling. Accordingly, pharmacological inhibition or genetic reduction of Hck activity suppresses alternative activation of tumor-associated macrophages and the growth of colon cancer xenografts. Thus, Hck may serve as a promising therapeutic target for solid malignancies.

[*]Correspondence: robert.odonoghue@onjcri.org.au (R.J.J.O.), matthias.ernst@onjcri.org.au (M.E.).
[7]These authors contributed equally
[8]Lead Contact

SUPPLEMENTAL INFORMATION

Supplemental Information includes eight figures and one table and can be found with this article online at http://dx.doi.org/10.1016/j.ccell.2017.03.006.

AUTHOR CONTRIBUTIONS

Experimental Work, A.R.P., C.G.L., F.M., A.P., Y.K., G.L., L.B., L.W., C.T., S.M., T.L.P., and R.J.J.O'D; Data Interpretation, A.R.P., C.G.L., F.M., S.M., L.W., O.S., C.L., T.L.P., R.J.J.O'D., and M.E.; Writing of Manuscript, A.R.P., R.J.J.O'D., and M.E.; Study Conception, A.R.P., G.L., R.J.J.O'D., and M.E.; Funding, O.S., R.J.J.O'D., and M.E.

Graphical abstract

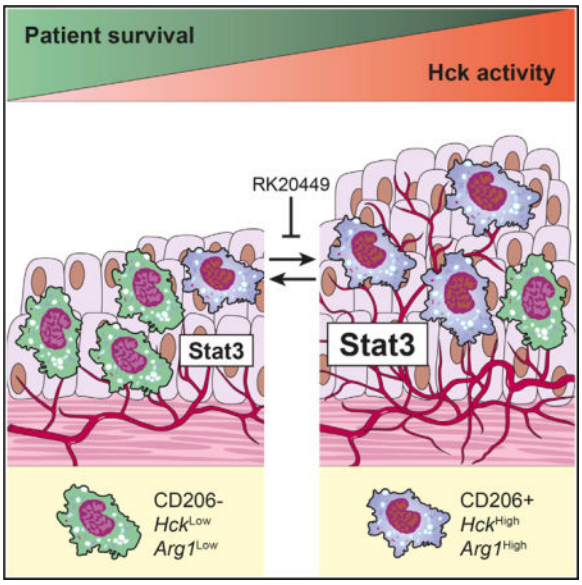

INTRODUCTION

The cytoplasmic hematopoietic cell kinase (HCK) is one of nine SRC family non-receptor tyrosine kinases (SFKs) and is expressed primarily in cells of the myeloid and B lymphocyte lineages (Ziegler et al., 1987). The physiological functions of Hck have been delineated in mice either completely deficient for Hck expression (Hck^{KO}) (Lowell and Benton, 1998), or in Hck^{CA} mice expressing a constitutive active kinase encoded by a mutation in the endogenous *Hck* gene (Ernst et al., 2002). These studies suggest a regulatory role for Hck during innate immune responses, with Hck^{CA} mice showing enhanced migration of myeloid cells resulting in exacerbated response to lipopolysaccharide (LPS) administration (Ernst et al., 2002).

Owing to a common molecular structure, aberrant activation of SFKs most frequently results from truncation or phenylalanine missense mutation of the C-terminal located negative regulatory tyrosine residue (Y499 in mouse Hck), which was first recognized as the molecular mechanism bestowing oncogenic activity to the viral oncoprotein v-Src (Snyder and Bishop, 1984). Subsequent studies have identified similar mutations in the cellular counterpart c-SRC, including somatic truncation mutations in 12% of advanced human colon colorectal cancer (CRC) (Irby et al., 1999). Likewise, hematopoietic malignancies can occur from aberrant HCK activation as a consequence of de novo formation of oncogenic HCK fusion proteins, or expression of viral proteins that impair the catalytic regulation of HCK activity (Pene-Dumitrescu et al., 2012). Increased *HCK* expression is also associated with breast, gastric, and other solid malignancies (Kubo et al., 2009; Rody et al., 2009), and a transcriptome survey of human CRC xenografts grown in mice identified *Hck* as the most abundantly expressed SFK in the tumor-associated host stroma (Isella et al., 2015).

The tumor stroma comprises a heterogeneous collection of cells including fibroblasts, adipocytes, endothelial and mesenchymal cells, together with cells of the adaptive and innate immune systems. Among the latter, macrophages and other myeloid-derived cells promote tumorigenesis through the secretion of growth factors and cytokines that enhance angiogenesis, stimulate tumor cell survival, invasion, and metastasis, and confer immune evasion (Lanskron et al., 2014). Some of these cells undergo polarization within the tumor microenvironment in response to cues from tumor cells and activated lymphocytes. For neutrophils, myeloid-derived suppressor cells and best characterized for macrophages (Mantovani, 2014), this encompasses a phenotypic continuum from M1-like, classically activated macrophages (CAMs) with phagocytic activity to M2-like, alternatively activated macrophages (AAMs) associated with wound-healing and tissue-repair responses (Qian and Pollard, 2010). Accordingly, interferon gamma and tumor necrosis factor alpha (TNF-α) induce polarization toward CAM endotypes associated with tumoricidal responses, and characterized by the induction of NOS2 and the release of inflammatory cytokines. In contrast, the Th2-derived cytokines, interleukin-4 (IL-4) and IL-13 promote polarization toward AAM endotypes associated with the induction of Arg1 to collectively promote angiogenesis, tissue remodeling and immune suppression (Biswas and Mantovani, 2010).

We previously observed that exacerbation of inflammatory signaling and enhanced immune cell recruitment in *Hck*^{CA} mice resulted in spontaneous innate immune cell consolidation in the lung that was reminiscent of chronic obstructive pulmonary disease, and infrequently triggered formation of pulmonary adenocarcinoma (Ernst et al., 2002). Because of the striking expression of HCK in the non-epithelial stromal compartment of colon cancer xenografts, we here determined the mechanism by which Hck signaling in immune cells promotes inflammation and tumor formation.

RESULTS

Excessive *HCK* Expression in Human CRC Is Associated with an AAM Gene Signature

HCK is the most abundantly expressed SFK in the stroma of mice bearing human CRC xenografts (Isella et al., 2015), but the functional relevance of this observation remains unclear. We therefore used the tyrosine-phosphorylated protein isoforms as surrogate markers for HCK activity in matched human CRC and control biopsies, and observed increased abundance of the phosphorylated (p)-p59HCK and p-p61HCK protein isoforms in three of seven tumors (Figure 1A). This observation correlated with elevated *HCK* mRNA expression in these biopsies ($r = 0.8$, $p = 0.048$) (Figure 1B). In these tumors, we confirmed that HCK protein localized to stromal cells co-expressing the leukocyte common antigen CD45, but not to EpCAM^{+} epithelial cells (Figure 1C).

We next defined the median level of *HCK* gene expression in two independent datasets (GEO: GSE16125, GSE17537) to categorize human CRC samples into *HCK*^{High} and *HCK*^{Low} cohorts (Goswami and Nakshatri, 2013). Surprisingly, we identified a poorer overall survival for the *HCK*^{High} cohorts (Figure 1D). We next mined TCGA transcriptome datasets by Voom differentially expressed gene analysis and identified 864 genes with at least a 2-fold difference in expression between *HCK*^{High} and *HCK*^{Low} sporadic CRC tumors (844 upregulated, 20 down-regulated, $p < 0.05$). Because HCK may regulate gene expression

in alternatively activated human monocytes (Bhattacharjee et al., 2011), we interrogated the expression signatures of the *HCK*^{High} and the *HCK*^{Low} CRC cohorts for genes associated with AAMs and CAMs. We used transcriptional profiling studies from polarized monocytes (Kadl et al., 2010; Lacey et al., 2012) as a guide to identify CAM- and AAM-associated genes that were at least 2-fold more abundant ($p < 0.05$) in the *HCK*^{High} than the *HCK*^{Low} cohort. Among the 100 most differentially expressed genes, 39 were associated with an AAM and 25 with a CAM endotype (Figure 1E). When subjected to KEGG pathway analysis, the *HCK*^{High} gene expression set revealed enrichments for pathways associated with asthma, rheumatoid arthritis, leishmaniasis, and other AAM-linked diseases (Table S1).

Given the overlapping activity among SFKs, we next sought to identify AAM and CAM genes associated with the four SFKs most prominently expressed in the mouse stroma of human CRC xenografts (Isella et al., 2015). Using a similar strategy to that for sub-dividing patients according to *HCK* expression, we identified CAM- and AAM-associated markers from the top 100 upregulated genes for the *FGR*, *LCK*, and *LYN* cohorts (Figure S1A). Interestingly, the *HCK*^{High} group contained by far the largest number of AAM-associated genes, while the *LYN*^{High} cohort contained the most CAM-associated genes. We then selected *IL7R, HLA-DQA1, PLEK*, and *IGSF6* for CAM, and *F13A1, C3AR1, C1QB*, and *SLAMF8* for AAM genes overexpressed in *HCK*^{High} tumors, alongside *IDO1* and *MARCO* as CAM and AAM genes regulated by all four SFKs, and confirmed their differential expression between *HCK*^{High} and *HCK*^{Low} CRC tumors analyzed in Figure 1A by qPCR (Figure S1B). Collectively, this provides a strong correlation between *HCK* gene expression, HCK activation, and expression of an AAM signature associated with poor patient prognosis.

Constitutive Hck Activity Enhances Sporadic and Colitis-Associated CRC Associated with Increased Stat3 Activity

To investigate a functional link between excessive HCK activity and CRC, we exploited *Hck*^{CA} mutant mice, which carry a homozygous tyrosine-to-phenylalanine ($Y_{499}F$) substitution mutation in the endogenous Hck protein to render the kinase constitutively active (Ernst et al., 2002). We subjected *Hck*^{CA} mutant mice to a model of sporadic colon tumorigenesis by repeated administration of the carcinogen azoxymethane (AOM). In a complementary model, we also used AOM in conjunction with exposure two cycles of dextran sodium sulfate to replicate the inflammation flares observed in colitis-associated colon cancer (CAC). In the sporadic CRC model we reproducibly detected at least twice as many tumors in *Hck*^{CA} mice compared with wildtype (WT) mice, and those tumors were consistently larger (Figures 2A and 2B). This observation was also replicated in the CAC model (Figures S2A and S2B). We then quantified the phosphorylated protein isoforms of Stat3, Erk, and rpS6 as surrogates for activation of pathways underpinning CRC growth (Putoczki et al., 2013; Thiem et al., 2013) and observed prominent Stat3 and rpS6 phosphorylation in tumors from *Hck*^{CA} mice in either model (Figures 2C and S2C), while the excessive Erk pathway remained restricted to tumors of CAC-challenged *Hck*^{CA} mice (Figure S2C). Because we previously showed that Gp130-family cytokines facilitates the growth of CRC tumors (Thiem et al., 2013), we analyzed expression of the genes encoding IL-6 and IL-11, and detected elevated expression of both cytokines in sporadic and CAC

tumors of *Hck*^{CA} mice (Figures 2D and S2D). We therefore conclude that irrespective of the presence of overt colitis, excessive Hck activity promotes tumor incidence/initiation as well as tumor growth/progression, and this correlates with activation of signaling pathways engaged by IL-6 and IL-11 (Bollrath et al., 2009; Putoczki et al., 2013).

Hematopoietic *Hck*^{CA} Promotes Tumorigenesis

To investigate the cellular fraction that conferred increased susceptibility of *Hck*^{CA} mice to tumorigenesis, we enriched for CD45^{+}CD11b^{+}F4/80^{+} tumor-associated macrophages (TAMs) and EpCAM^{+} tumor epithelial cells to confirm that HCK expression remained restricted to TAMs (Figures 3A and S3A). We then derived reciprocal bone marrow chimeras and controlled for confounding whole-body irradiation effects with syngeneic *Hck*$^{\leftarrow Hck}$ (Recipient$^{\leftarrow Donor}$) and WT$^{\leftarrow WT}$ chimeras. We observed a larger tumor burden in WT$^{\leftarrow Hck}$ bone marrow chimeras subjected to either the sporadic or the CAC tumorigenesis protocol (Figures 3B, 3C, S3B, and S3C), while the tumor burden in *Hck*$^{\leftarrow WT}$ mice remained similar to that of WT$^{\leftarrow WT}$ controls. Western blot analysis of sporadic and CAC tumors from *Hck*$^{\leftarrow Hck}$ and WT$^{\leftarrow Hck}$ mice revealed elevated Stat3 and rpS6 activity when compared with WT$^{\leftarrow WT}$ and *Hck*$^{\leftarrow WT}$ mice, while elevated p-Erk1/2 remained specific to CAC tumors from mice harboring *Hck*^{CA} bone marrow (Figures 3D and S3D).

Given the expression of HCK in the myeloid and B lymphoid cells, and the recognized crosstalk between lymphoid- and myeloid-derived immune cells during CRC progression (DeNardo et al., 2010), we exploited mature B and T lymphocyte-deficient *Rag1* knockout mice (*Rag1*^{KO}). Although we confirmed that *Rag1*^{KO} mice were resistant to AOM-induced sporadic tumorigenesis (Becker et al., 2004), we observed similar tumor burden between WT and *Hck*^{CA};*Rag1*^{KO} mutants in both models, although *Hck*^{CA};*Rag1*^{KO}mice harbored larger tumors (Figures 3E and S3E). Thus, constitutive Hck activation in the non-lymphoid bone marrow cell compartment boosts tumor initiation and growth.

Hck^{CA} Tumors Harbor AAMs

Since Hck activity enhances migration of immune cells to sites of inflammation (Ernst et al., 2002; Mazzi et al., 2015), we quantified tumor-associated immune cells by flow cytometry. Surprisingly, in both CRC models we observed a comparable abundance between WT and *Hck*^{CA} mice of CD45^{+} cells gated for CD19^{+} B lymphocytes (15.90% ± 0.93% versus 14.93% ± 0.73%; data refer to sporadic model), TCRβ^{+} T lymphocytes (36.87% ± 1.88% versus 33.73%±1.53%),orCD11b^{+}F4/80^{+}macrophages (17.8% ± 0.50% versus 19.36% ± 2.67%).

Since Hck signaling has been suggested to facilitate polarization of monocytes to an alternatively activated endotype (Bhattacharjee et al., 2011), we assessed the AAM markers *Il4*, *Il10*, *Il13*, *Arg1*, and *Ym1*, and CAM markers *Il1β*, *Tnfα*, *Nos2*, and *Cd86* in tumors from WT and *Hck*^{CA} mice (Figures 4A and S4A). Although AAM markers were more abundantly expressedintumors than in unaffected areas, we detected more profound AAM polarization in tumors of *Hck*^{CA} mice, and in particular of the functional AAM-determinant *Arg1* when compared with its CAM-counterpart *Nos2*. In *Hck*^{CA} tumors we also noted a further increase of *Il1β* and *Tnfα* expression, while tumor-free colon regions of these mice

showed also elevated expression of *Arg1* and *Ym1* (Figures 4A and S4A). Since we did not detect any difference in gene expression between colons of treatment-naive WT and Hck^{CA} mice, AAM polarization may occur through long-range signals from tumor cells rather than from their physical association with each other. These data mirror the prominent AAM signature in human HCK^{High} tumors and indicate that Hck activation promotes polarization toward an AAM endotype, rather than conferring quantitative changes to the various tumor-infiltrating immune cell populations.

Hck Activation Promotes Alternative Activation of TAMs

Next, we used CD206 expression in purified $CD45^+CD11b^+F4/80^+$ cells to identify AAMs, and confirmed their preferential accumulation in tumors of Hck^{CA} mice (Figures 4B and S4B). This coincided with purified $CD45^+CD11b^+F4/80^+$ TAMs in Hck^{CA} mice expressing higher levels of the AAM markers *Il4*, *Il10*, *Il13*, *Arg1*, *Ym1*, and *Tie2* than those isolated from tumors of WT mice (Figures 4C and S4C). We then performed reciprocal bone marrow transfer experiments to prove that the macrophage endotype was an intrinsic consequence of cells expressing the Hck^{CA} mutation. When compared with purified $CD45^+CD11b^+$ $F4/80^+$ TAMs from $Hck^{\leftarrow WT}$ and $WT^{\leftarrow WT}$ chimeras, the corresponding cells isolated from $WT^{\leftarrow Hck}$ mice in either CRC model retained elevated expression of *Il1β*, *Tnfa*, *Il4*, *Il13*, *Il10*, *Arg1*, *Ym1*, and *Tie2* observed in $Hck^{\leftarrow Hck}$ mice (Figures 4D and S4D).

Excessive Hck Activation Mediates Tumor-Promoting AAM Polarization through a Non-canonical Signaling Mechanism

Given the capacity of TNF-α to promote inflammation and tumor-igenesis in the CAC model (Popivanova et al., 2008), and the profound *Tnfa* expression in Hck^{CA} TAMs reminiscent of the exaggerated LPS-dependent TNF-α production by alveolar macrophages (Ernst et al., 2002), we constructed $Hck^{CA};Tnfa^{KO}$ mice. Surprisingly, these compound mutant mice exhibited a similar tumor burden as Hck^{CA} mice in either model, despite $Tnfa^{KO}$ mice remaining tumor free in both models (Oshima et al., 2014; Popivanova et al., 2008) (Figures 5A and S5A). Indeed, $Hck^{CA};Tnfa^{KO}$ mice had larger tumors than all other cohorts, consistent with the notion that increased *Tnfa* expression may limit tumor progression (Craven et al., 2015). However, TNF-α is unlikely to affect macrophage polarization in Hck^{CA} mice, because tumors from $Hck^{CA};Tnfa^{KO}$ and Hck^{CA} animals harbored both an AAM signature (Figures 5B and S5B).

To further clarify the contribution of the Th2 cytokines IL-4 and IL-13 to macrophage polarization in Hck^{CA} mice, we impaired intracellular signaling response to these cytokines by generating $Hck^{CA};Stat6^{KO}$ mice. Surprisingly, these mice still developed significantly more tumors than WT littermates, albeit fewer than observed in Hck^{CA} mice and retained elevated AAM gene expression (Figures 5C, 5D, S5C, and S5D). While $Stat6^{KO}$ mice remained completely protected from sporadic CRC development, the tumor burden of CAC-challenged $Stat6^{KO}$ mice was attenuated compared with WT mice, consistent with Stat6 deficiency enhancing tumor immunity in mice (Ostrand-Rosenberg et al., 2000). Thus, Hck^{CA} myeloid cells retain an AAM phenotype through non-canonical, IL-4/IL-13-independent signaling mechanisms, and these cells are further polarized in the context of colitis and mediate tumor formation independently of TNF-α.

Therapeutic Inhibition of Hck Antagonizes Tumor Progression in Mice

To translate the findings from *Hck*^{CA} mice to a clinically relevant setting, we first confirmed a prominent role for macrophages in Hck-driven cancer by limiting expression of the macrophage colony-stimulating factor receptor (encoded by the *Cfms* gene) in *Hck*^{CA} mice. We then established syngeneic MC38 CRC allografts in the corresponding *Hck*^{CA};*Cfms*$^{+/-}$ mice, and noted significantly smaller tumors in these hosts than in their *Hck*^{CA};*Cfms*$^{+/+}$ littermates (Figure 6A). This coincided with reduced abundance of F4/80^{+} macrophages in the tumors of *Hck*^{CA};*Cfms*$^{+/-}$ mice (Figure S6A). Likewise, *Hck*^{KO} mice had significantly smaller MC38 allograft tumors than WT hosts, thereby genetically confirming that ablation of *Hck* conferred an anti-tumor effect (Figure 6B).

Next, we exploited the HCK-specific pyrrolo-pyrimidine derivative RK20449, which kills stem cells required for the growth of acute myeloid leukemia xenografts (Saito et al., 2013). Accordingly, RK20449 also suppressed proliferation of the acute monocytic leukemia cell lines MOLM-13 and MV4-11, but not of MC38 CRC cells (Figure S6B), in which we could not detect *Hck* transcripts by qPCR analysis (data not shown). We then treated WT mice with palpable MC38 tumors and observed significantly smaller tumors with less phosphorylated Hck in the RK20449-treated cohort than in those treated with the biologically inactive stereoisomer or vehicle (Figures 6C and S6C). Because RK20449 administration did not affect tumor burden of MC38 allografts inoculated in *Hck*^{KO} hosts (Figure 6B), we surmise that the effect of RK20449 is mediated primarily through Hck inhibition in the host.

Pharmacological inhibition of Hck with RK20449 did not alter the infiltration of hematopoietic CD45^{+} cells or F4/80^{+} macrophages, but reducedtheabundanceofCD206^{+} cells,proliferating BrdU^{+} cells, and CD31^{+} endothelial cells (Figures 6D and S6D), which correlated with reduced expression of the AAM genes *Il4*, *Il10*, *Il13*, *Arg1*, and *Ym1*, but minimal effects on the CAM genes *Il1β*, *Tnfα*, and *Nos2* (Figure 6E). We also observed a similar reduced AAM gene expression in *Hck*^{KO} hosts, which was not further exaggerated in RK20449-treated *Hck*^{KO} hosts (Figure 6F), and RK20449 treatment did not further diminish BrdU^{+} MC38 cells in allografts in *Hck*^{KO} mice (Figure S6E).

We then used the human CRC cell lines HCT116, DLD1, and SW480, which do not express Hck and remained refractory to RK20449-dependent inhibition of growth (Figure S7A), to established subcutaneous tumors in immune-compromised *Rag1*^{KO} mice. After 10 days of systemic treatment with RK20449, we observed significantly smaller xenografts in RK20449-treated hosts compared with control cohorts (Figure 7A). Moreover, tumorsfromRK20449-treated micecontained less of the activated p56Hck and p59Hck isoforms, but not of the corresponding phosphorylated isoforms of p60Src or p53Lyn (Figure 7B).We also observed reduced expression of AAM genes in the xenografts grown in RK20449-treated mice (Figure S7B), consistent with a smaller proportion of CD206^{+} TAMs and Ki67^{+} proliferating cells in these xenografts (Figures 7C and S7C).

Hck Mediates Induction of the AAM Endotype Independently of Stat3

While in sporadic and CAC tumors most p-Stat3 remained within the mucosal epithelium, we observed limited co-localization between p-Stat3 and Hck in hematopoietic cells (Figure 8A). Consistent with our observation that IL-6/IL-11 stimulation resulted in a small, but significant induction of *Arg1*, but not of *Nos2*, expression in macrophages (Figure 8B), others proposed that Stat3 can promote an AAM endotype by cooperating with Stat6 (Stritesky et al., 2011), or possibly through mechanisms that involve the Stat3 target gene *cMyc* (Pello et al., 2012). In Hck^{CA} TAMs we confirmed a marked increase in the Stat3 target genes *Socs3* and *cMyc*, as well as of the angiogenic *cMyc* target genes *Vegfa*, *Hif1a*, and *Tgfβ*, and of the Stat3-activating cytokines *Il6* and *Il11* (Figure 8C). Because Stat3 can also be activated by non-receptor-associated tyrosine kinases (Guryanova et al., 2011), we determined Stat3 activity in naive bone marrow-derived macrophages (BMDM). While p-Stat3 remained comparable between WT, Hck^{CA}, and Hck^{KO} BMDMs (Figure 8D), these cells already showed differential expression of the AAM markers that matched their *Hck* genotype (Figure 8E). Consistent with Hck activity being functionally uncoupled from Stat3 activity during AAM polarization, we found that inhibition of Stat3, either genetically in WT cells or pharmacologically with Stattic in Hck^{CA} cells, neither inhibited Th2 cytokine-induced AAM polarization in WT cells nor AAM polarization of Hck^{CA} cells (Figure 8F). From these collective observations, we surmise that Hck-mediated Th2-cytokine/Stat6-independent AAM polarization occurs also largely independent of Stat3.

Having observed a pronounced angiogenic expression signature in $F4/80^+$ TAMs on Hck^{CA} tumors (Figures 4C, S4C, and 8C), we found more $Tie2^+F4/80^+$, as well as $Tie2^+F4/80^-$ cells in sporadic and CAC tumors of Hck^{CA} mice than of WT mice (Figure S8A). Indeed, the more abundant CD31 staining in tumors of Hck^{CA} mice (Figure S8B) suggests that excessive Hck activity may increase tumor burden in part by enabling endothelial cell expansion.

DISCUSSION

Here we provide evidence for dysregulated SFK activity in the tumor microenvironmentas adriver for solid tumor growth. We correlate these findings with an AAM endotype-biased expression signature of TAMs, reduced tumor burden in Hck^{CA} mice following adaptive transfer of WT bone marrow, and diminished CRC allograft growth in WT hosts treated with a Hck kinase inhibitor. These functional findings are consistent with our observation that increased HCK activity in CRC biopsies correlated with an AAM-biased expression profile, a poorer survival of patients with high *HCK* expression, and our observation that therapeutic inhibition of stromal Hck suppressed the growth of human CRC xenografts.

Many immune cells undergo an endotypic change by switching from their host defense function to an “alternatively activated” tissue-repair program that promotes tumor growth and progression (Qian and Pollard, 2010). Accordingly, IL-4 (DeNardo et al., 2009; Gocheva et al., 2010), IL-10 (Lang et al., 2002), and immunoglobulin signaling through Fcγ receptors (Andreu et al., 2010) confers AAM polarization. Likewise, mucosal-derived IL-13, $CD4^+$ T cells (Pedroza-Gonzalez et al., 2011), and CD1d-restricted NKT cells (Terabe et al., 2003) also confer TAM polarization. Our observations suggest that Hck^{CA} myeloid cells

promote tumor initiation (resulting in more tumors), In addition, the Tie2 endotype displayed by TAMs in *Hck*^{CA} mice, the more extensive vascularization of tumors in *Hck*^{CA} mice, and a converse, albeit very moderate reduction of CD31^{+} cells in tumors of *Hck*^{KO} hosts, may provide a mechanism by which Hck promotes tumor progression.

IL-4 and IL-13, as the predominant AAM-inducing cytokines, are overexpressed in TAMs of *Hck*^{CA} mice. However, neither expression of the prototypical AAM markers *Il10* and *Arg1*, nor the increased tumor burden in *Hck*^{CA} mice, required Stat6, the common signal transducer engaged by IL-4 and IL-13. These observations are surprising, since *Stat6*^{KO} mice are protected against IL-4/IL-13-mediated type 2 immune responses (Kuperman et al., 1998; Stamm et al., 1998; Yokozeki et al., 2000), and suggest that the TAM endotype in *Hck*^{CA} mice is unlikely to be mediated by CD4^{+} cell-derived Th2-cytokines. However, non-canonical pathways for AAM development have been associated with c-Myc and Stat3. In human macrophages, for instance, c-MYC and PPAR-γ expression enhance the AAM endotype (Pello et al., 2012). On the other hand, Stat3 may interact with, or substitute for Stat6 (Stritesky et al., 2011), consistent with findings that Stat3 activation within immune cells is more pronounced in colitis-associated cancer than in dysplastic or normal colon tissues, where p-Stat3 and p-Stat6 show a reciprocal relationship (Wick et al., 2012). Thus, our results suggest that the elevated abundance of IL-6/IL-11 in CRC (Putoczki et al., 2013) may further promote AAM polarization irrespective of the Hck activation status in these cells. By contrast, Stat3 activity in the neoplastic epithelium, triggered by CD45^{+} leukocyte and EpCAM^{+} epithelial cell-derived IL-11 (Putoczki et al., 2013), drives excessive proliferation of colorectal tumor cells as long as signaling through the mTorc/rpS6 pathway is not rate limiting (Thiem et al., 2013).

Our data suggest a mechanism whereby Hck signaling elicits an AAM endotype possibly through its physical association with the Fcγ receptor and the Gp130 receptor subunit shared among the IL-6 family cytokines (Crowley et al., 1997; Ernst et al., 1994; Schaeffer et al., 2001). Thus, the abundantly expressed IL-6/IL-11 cytokines in the tumors of *Hck*^{CA} mice may provide an autocrine/paracrine mechanism to prime or stabilize an AAM endotype characterized by excessive production of TNF-α, vascular endothelial growth factor, and IL-10 (Wang et al., 2010), and which may be further enforced by Fcγ receptor activation in response to B lymphocyte-secreted IgG complexes. Such a mechanism is consistent with BMDMs from *Hck*^{CA} mice intrinsically displaying an AAM endotype. Furthermore, constitutive Hck activity may also short-circuit Fcγ receptor signaling in *Hck*^{CA};*Rag*^{KO} mice to promote AAM polarization and tumor formation.

The extensive sequence similarities among SFK members underpins functional redundancies and minimal phenotypes in mice individually lacking Hck (reduced macrophage phagocytosis in vitro), Fgr (no overt phenotype in mice), or Yes (no overt phenotype in mice) (Lowell et al., 1994; Stein et al., 1994). Although Hck and Fgr only show overlapping localization at the cell membrane, compound *Hck*^{KO};*Fgr*^{KO} mice are unable to clear *Listeria* infection (Lowell et al., 1994), and show blunted recruitment of myeloid cells to arterial plaques or to LPS-challenged lungs (Mazzi et al., 2015; Medina et al., 2015). By contrast, excessive activation of endogenous SFK results in a lethal autoimmune response in *Lyn*^{CA} mice (Hibbs et al., 1995) and inflammatory lung disease in *Hck*^{CA} mice (Ernst et al., 2002).

The latter phenotype can be rationalized by the presence of Wasp, Cbl, paxilin, and other Hck substrates in adhesion and migration complexes (Poh et al., 2015), and the capacity of Hck to mediate β1/2 integrin-dependent outside-in signaling and to facilitate the formation of podosomes (Kovács et al., 2014). However, we note that despite the more aggressive growth of tumors in *Hck*^{CA}, the extent of TAMs remained comparable. This observation is consistent with reports that the extent of macrophage infiltration is not predictive for long-term survival of CRC patients, but more likely to correlate with the TAM endotypes (Bailey et al., 2007; Edin et al., 2012).

Targeting the genetically more stable cells of the tumor microenvironment, possibly in conjunction with therapies tailored against tumor-driving mutations, provides a strategy to lessen the resistance afforded by acquisition of mutations in genetically less-stable tumor cells. Accordingly, multiple approaches for targeting macrophages are pursued, including blocking of tumor-derived factors that recruit monocyte-derived macrophages, inhibiting macrophage function, or selectively targeting TAMs to decrease their viability (Germano et al., 2013). Conceptually more attractive are manipulations to “re-educate” macrophages by reducing their tumorigenic AAM profile in favor of reactivating a tumoricidal CAM program. Indeed, recent approaches to block CSF1 receptor signaling resulted in re-polarization of TAMs toward a CAM endotype, and increased survival in a mouse model of glioma (Pyonteck et al., 2013). However, CSF1 blockade may also cause systemic suppression of all macrophage endotypes (Ries et al., 2014; Ruffell et al., 2014). Inhibition of PI3K γ/δ kinases may also suppress expression of genes associated with wound healing and AAMs (Balakrishnan et al., 2015; Kieckbusch et al., 2015), although their deficiency distorts T cell development and can cause multiple organ failure (Ji et al., 2007). By contrast, our data strongly suggest that targeting of HCK would selectively suppress AAM endotypes, while in its complete absence the phagocytic activity of macrophages is retained in *Hck*^{KO} mice and prevents the development of detrimental phenotypes (Lowell et al., 1994). Dasatinib and other approved pan-SFK inhibitors could therefore confer a beneficial effect to cancer patients with excessive *HCK* activity in the tumor microenvironment or indeed in epithelia, as a mechanism likely to confer a chemotherapy-tolerant state to breast cancer cells (Goldman et al., 2015). The availability of crystal structures for inhibitor-bound SFKs (Schindler et al., 1999) should allow for the rapid development of inhibitors with superior properties than RK20449.

STAR*METHODS

Detailed methods are provided in the online version of this paper and include the following:

KEY RESOURCES TABLE

REAGENT or RESOURCE	SOURCE	IDENTIFIER
Antibodies		
IRDye Goat anti-rabbit secondary antibody	LICOR Bio-sciences	Cat#926-32221; RRID: AB_621841
IRDye Goat anti-mouse secondary antibody	LICOR Bio-sciences	Cat#926-32210; RRID: AB_621842

REAGENT or RESOURCE	SOURCE	IDENTIFIER
Mouse anti-mouse Actin	Sigma	Cat#A1978; RRID: AB_476692
Rabbit anti-mouse p-Stat3 (Tyr-705)	Cell Signaling	Cat#9145; RRID: AB_2491009
Rabbit anti-mouse Stat3	Cell Signaling	Cat#4904; RRID: AB_331269
Rabbit anti-mouse pErk 1/2 (Thr-202/ Tyr-204)	Cell Signaling	Cat#9101; RRID: AB_331646
Rabbit anti-mouse Erk1/2	Cell Signaling	Cat#4695; RRID: AB_390779
Rabbit anti-mouse p-rpS6 (Ser-240/244)	Cell Signaling	Cat#2215; RRID: AB_331682
Rabbit anti-mouse rpS6	Cell Signaling	Cat#2217; RRID: AB_331355
Rabbit anti-mouse pHck (Tyr-410)	Abcam	Cat#61055; RRID: AB_942255
Mouse anti-mouse Hck	Santa Cruz	Cat#G-4; RRID: AB_1122638
Rabbit anti-mouse p-Src (Tyr-527)	Cell Signaling	Cat#2105; RRID: AB_331034
Rabbit anti-mouse Src	Cell Signaling	Cat#2108; RRID: AB_10695298
Rabbit anti-mouse p-Lyn (Tyr-507)	Cell Signaling	Cat#2731; RRID: AB_2138262
Rabbit anti-mouse Lyn	Cell Signaling	Cat#2732; RRID: AB_10694080
Mouse anti-mouse BrdU	BD Biosciences	Cat#555627; RRID: AB_10015222
Rat anti-mouse CD45	BD Biosciences	Cat#553076; RRID: AB_394606
Rat anti-mouse F4/80	Abcam	Cat#6640; RRID: AB_1140040
Rabbit anti-mouse CD31	Abcam	Cat#28364; RRID: AB_726362
Mouse anti-human Ki67	DAKO	Cat#GA626
Anti-rat Alexa-Fluor 488	Invitrogen	Cat#A-11006; RRID: AB_141373
Anti-mouse Alexa-Fluor 594	Invitrogen	Cat#A-11032; RRID: AB_141672
Anti-rabbit Alex-Fluor 647	Invitrogen	Cat#A-21443
Rabbit anti-mouse Tie2	Abcam	Cat#24859; RRID: AB_2255983
Mouse anti-mouse p-Stat3 (Tyr-705)	Cell Signaling	Cat#4113; RRID: AB_2198588
Rabbit anti-human HCK	Cell Signaling	Cat#14643
Mouse anti-human EpCAM	Cell Signaling	Cat#VU1D9; RRID: AB_2098657
Mouse anti-human CD45	DAKO	Cat#GA751
FITC rat anti-mouse EpCAM + isotype control	BioLegend	Cat#118208; RRID: AB_1134107, #400208; RRID: AB_326456
APC rat anti-mouse CD19 + isotype control	BioLegend	Cat#115512; RRID: AB_313647, #400512; RRID: AB_326534
PE hamster anti-mouse TCRβ + isotype control	BioLegend	Cat#109208; RRID: AB_313431, #400908; RRID: AB_326594
PE rat anti-mouse CD11b + isotype control	BD Biosciences	Cat#553311, #553989
APC-Cy7 rat anti-mouse CD45.2 + isotype control	BioLegend	Cat#109824; RRID: AB_830789, #400230; RRID: AB_326478
PE-Cy7 rat anti-mouse F4/80 + isotype control	BioLegend	Cat#123114; RRID: AB_893478, #400522; RRID: AB_326542
APC rat anti-mouse CD206 + isotype control	BioLegend	Cat#141708; RRID: AB_10900231, #400512; RRID: AB_326534
Biological Samples		

REAGENT or RESOURCE	SOURCE	IDENTIFIER
De-identified matched human sporadic colorectal cancer samples	The Royal Melbourne Hospital	N/A
Chemicals, Peptides, and Recombinant Proteins		
Azoxymethane	Sigma	Cat#A5486
Dextran Sodium Sulfate	MP Biomedicals	Cat#02160110
Baytril	Baytril	N/A
BrdU	Amersham Biosciences	Cat#RPN201
RK20449	Calderwood et al., 2002, Saito et al., 2013	N/A
TRIzol	Life Technologies	Cat#15596026
Diaminobenzine (DAB)	DAKO	Cat#K3468
ProLong® Gold Antifade Mountant with DAPI	Thermo Fisher	Cat#P36931
Recombinant mouse IL4	Peprotech	Cat#214-14
Recombinant mouse IL13	Peprotech	Cat#210-13
Recombinant mouse IL6	Peprotech	Cat#216-16
Recombinant mouse IL11	Peprotech	Cat#220-11
Stattic	Cayman Chemical	Cat#14590
Collagenase/Dispase	Roche	Cat#10269638001
DNase I	Roche	Cat#10104159001
Captisol	Captisol	N/A
Critical Commercial Assays		
RN-easy Mini Plus kit	Qiagen	Cat#74136
High Capacity cDNA Reverse Transcription kit	Applied Biosystems	Cat#4368813
SensiMix SYBR kit	Bioline	Cat#QT605-20
Taqman® Real-Time PCR Master mix	Life Technologies	Cat#4304437
Avidin Biotin Complex ABC-kit with biotinylated secondary antibodies	Vector Laboratories	Cat#PK6101, 6102, 6104
Experimental Models: Cell Lines		
MC38	Prof. Frederic Hollande	
HCT116	Prof. Oliver Sieber	ATCC #CCL-247
DLD1	Prof. Oliver Sieber	ATCC #CCL-221
SW480	Prof. Oliver Sieber	ATCC #CCL-228
MOLM-13	Dr. Gabriela Brumatti	DSMZ #ACC-554
MV4-11	Dr. Gabriela Brumatti	DSMZ #ACC-102
Experimental Models: Organisms/Strains		
Wild-type C57BL/6 mice	WEHI	
Rag1 knock-out mice	Mombaerts et al., 1992	
HckCA knock-in mice	Ernst et al., 2002	
Hck knock-out mice	Lowell et al., 1994	

REAGENT or RESOURCE	SOURCE	IDENTIFIER
TNFa knock-out mice	Marino et al., 1997	
Stat6 knock-out mice	Takeda et al., 1996	
Cfms+/−	Dai et al., 2002	
Oligonucleotides		
Please refer to STAR Methods section “RNA extraction and qPCR.” for probe and primer details.		
Software and Algorithms		
GraphPad Prism Version 5	GraphPad Prism	www.graphpad.com
Flow Jo Version 10	FlowJo	www.flojow.com
Aperio ImageScope	Leica Biosystems	http://www.leicabiosystems.com/digital-pathology/digital-pathology-n
FIJI (ImageJ)	ImageJ	https://fiji.sc/
TCGA data portal	https://tcga-data.nci.nih.gov/tcga/	TCGA
R statistical package	http://www.rproject.org	Ver 3.2.1
Bioconductor (R packages Limma/ edgeR/GOseq)	http://bioconductor.org/	biocInstaller 1.184
Gene expression datasets GSE16125 and GSE17537	https://www.ncbi.nlm.nih.gov/geo	GEO

CONTACT FOR REAGENT AND RESOURCE SHARING

Further information and requests for resources and reagents shouldbe directed tothe Lead Contact, Matthias Ernst (Matthias.Ernst@ONJCRI.org.au).

EXPERIMENTAL MODEL AND SUBJECT DETAILS

Study Approval—All animal studies were approved and conducted in accordance with the Animal Ethics Committee of the Ludwig Institute for Cancer Research or the Walter and Eliza Hall Institute of Medical Research. Human colorectal tumor biopsies from de-identified patients were obtained with signed patient-informed consent and approval from the Human Ethics Review Committee of the Walter and Eliza Hall Institute.

Mice—All mice were bred on C57BL/6 genetic background and maintained in specific pathogen—free facilities at the Walter and Eliza Hall Institute of Medical Research or the Ludwig Institute for Cancer Research, Australia. Co-housed, sex-matched and age-matched WT, *Hck*^{CA} (Ernst et al., 2002), *Hck*^{KO} (Lowell et al., 1994), *Hck*^{CA};*Rag1*^{KO}, *Hck*^{CA};*Tnf*α^{KO}, *Hck*^{CA};*Stat6*^{KO}, *Hck*^{CA};*Cfms*$^{+/-}$ and their corresponding single allele *Rag1*^{KO} (Mombaerts et al., 1992), *Tnfa*^{KO} (Marino et al., 1997), *Stat6*^{KO} (Takeda et al., 1996) and *Cfms*$^{+/-}$ (Dai et al., 2002) controls were used.

Tumor Models—Sporadic colon cancer was induced by a single weekly intraperitoneal injection of azoxymethane (AOM, 10mg/kg, Sigma-Aldrich) for 6 consecutive weeks (Neufert et al., 2007). Mice were collected at 16 weeks following the last AOM injection. To model colitis-associated cancer, 6 week old mice received a single AOM injection followed by two cycles of dextran sodium sulphate (DSS)-supplemented drinking water (2% m/v,

MW 36–50kDa, MP Biochemicals) ad libitum for 5 days. The DSS cycles were interspersed with two weeks of normal drinking water. Mice were collected 8 weeks after the last DSS cycle.

The mouse MC38 CRC cell line was cultured in DMEM and 10% fetal calf serum. Six-week-old female C57BL/6 mice were inoculated subcutaneously with 1×10^6 MC38 cells into the left and right flanks. The human colon adenocarcinoma cell lines HCT116, DLD1 and SW480 and the human leukaemia cell lines MOLM-13 and MV4-11 were cultured in RPMI and 10% fetal calf serum. Six-week-old *Rag1*^{KO} mice were inoculated subcutaneously with 4×10^6 HCT116, DLD1 or SW480 cells into the left and right flanks. Once palpable tumors formed, mice were randomized into treatment groups. Tumor measurements were recorded by an independent assessor who was blinded to the experimental conditions.

METHOD DETAILS

Experimental Design—All experiments were performed atleast twice with aminimum of three age- and sex-matched mice per group. The specific n (number of animals) used per cohort is indicated in the respective figure legends. For RK20449 studies, mice with comparable tumor sizes were randomized into treatment groups. Tumor growth was measured and recorded by an independent assessor who was blinded to the experimental conditions.

Generation of Bone-Marrow Chimeras—Bone-marrow was harvested from the femurs and tibias of donor mice by flushing with sterile PBS. Recipient mice were lethally irradiated with 2 doses of 5.5 Gy γ-irradiation 3-hours apart, before receiving 5×10^6 donor bone marrow cells via tail vein injection. Mice were then maintained on antibiotic-supplemented water (Baytril™) for 3 weeks and complete bone marrow reconstitution was assessed 8 weeks later as described (Putoczki et al., 2013).

Tissue Collection—Two hours prior to euthanization, mice were given a single intraperitoneal injection of BrdU (Amersham Biosciences, 50mg/kg). Excised colons were flushed clear of feces with PBS, opened longitudinally and laid flat onto paper-towels and photographed. Prior to dissection, tumors were scored according to their size. Tumors and PBS-rinsed colons from treatment-naïve and tumor-bearing mice were either snap frozen for molecular analysis or fixed in 10% neutral buffered formalin overnight at 4°C for histological analysis.

In Vitro Cell Line Proliferation Assay—To determine proliferation of cancer cell lines in vitro, 10^5 cells were treated with RK20449 or 0.001% DMSO as vehicle for 48 hours. Cultures were then trypsinized and counted with a Countess II Automated Cell Counter (Invitrogen) following trypan blue exclusion staining.

RK20449 Treatment—RK20449 and its biologically inactive *cis*-stereoisomer (Saito et al., 2013) were synthesized as described (Calderwood et al., 2002), dissolved in 12% Captisol® and administered twice daily (i.p., 30mg/kg) for 7 (MC38 allograft model) or 10 days (HCT116, DLD1 and SW480 xenograft models).

Protein Extraction and Western Blot Analysis—Protein lysates from were prepared using the TissueLyser II (Qiagen) and RIPA lysis buffer containing protease- and phosphatase-inhibitor tablets (Roche). Protein concentration was determined by the bicinchoninic acid (BCA) assay. Thereafter, tissue homoge-nates were reconstituted in 4x Laemmli's loading buffer, resolved on 10% SDS-polyacrylamide gels and dry-transferred onto nitrocellulose membranes (Invitrogen). Membranes were incubated overnight at 4°C with the indicated primary antibodies, followed by incubation with fluorescent conjugated secondary antibodies for 1 hour (refer to Key Resources Table). Proteins were visualized using the Odyssey Infrared Imaging System (LI-COR Biosciences). Densitometry analysis was performed in FIJI (ImageJ) as described (Miller, 2010).

RNA Extraction and qPCR—RNA extraction from whole tissues and FACs sorted macrophages was performed as described (Putoczki et al., 2013; Thiem et al., 2013), using TRIzol (Life Technologies) according to the manufacturer's instructions. RNA extraction on FACS purified cells was performed using the RN-easy Mini Plus kit (Qiagen). RNA(2μg) was used to generate cDNA with the High Capacity cDNA Reverse Transcription Kit (Applied Biosystems) according to the manufacturer's instructions. Quantitative RT-PCR analysis was performed on duplicate samples with SensiFAST SYBR kit (Bioline) or Taqman® Real-Time PCR Master mix (Life Technologies) using the Viia7 Real-Time PCR System (Life Technologies) over 40 cycles (95°C for 15s, 60°C/1min) and following an initial denaturation step at 95°C/10min. *18S, Gapdh* or *ACTIN* were used as house-keepers and fold changes in gene expression were obtained using the 2-ΔΔCT method.

Taqman® probes used were human *ACTIN* (Hs01060665_g1), *HCK* (Hs01067403_m1), *IL7R* (Hs00233682_m1), *PLEK* (Hs00160164_m1), *HLA-DQA1* (Hs03007426_mH), *IGSF6* (Hs00175526_m1), *IDO1* (Hs00984148_m1), *F13A1* (Hs01114178_m1), *C1QB* (Hs00608019_m1), *SLAMF8* (Hs00975302_g1), *C3AR1* (Hs00269693_s1), *MARCO* (Hs00198935_m1) and mouse *Gapdh* (Mm99999915_g1), *Hck* (Mm01241463_m1), *Il6* (Mm00446190_m1), *Il11* (Mm00434162_m1), *Socs3* (Mm00545913_s1), *cMyc* (Mm00487804_m1), *Tgfβ* (Mm01178820_m1), *Vegfa* (Mm00437306_m1) and *Hif1α* (Mm00468869_m1) from ThermoFisher.

SYBR Green qPCR primers were purchased from Geneworks with the following sequences:

Gene	Forward 5-3′	Reverse 5-3′
18s	GTAACCCGTTGAACCCCATT	CCATCCAATCGGTAGTAGCG
Il1β	ACGGACCCCAAAAGATCAAGGGCT	CCTGGAAGGTCCACGGGAAAGAC
Tnfα	ACCCTCACACTCAGATCATC	GAGTAGACAAGGTACAACCC
Nos2	GCCACCAACAATGGCAACA	CGTACCGGATGAGCTGTGAATT
Cd80	CCATGTCCAAGGCTCATTCT	GGCAAGGCAGCAATACCTTA
Cd86	TCAGTGATCGCCAACTTCAG	TTAGGTTTCGGGTGACCTTG
Il4	CACAGGAGAAGGGACGCCATGC	ATGCGAAGCACCTTGGAAGCCC

Il10	GGTTGCCCAGCCTTATCGGA	ACCTGCTCCACTGCCTTGCT
Il13	GCTCTGGGCTTCATGGCGCT	AGGGCTACACAGAACCCGCCA
Arg1	AGGACAGCCTGGAGGAGGGG	TGGACCTCTGCCACCACACCAG
Ym1	GGGCATACCTTTATCCTGAG	CCACTGAAGTCATCCATGTC
Tie2	GGTTTTGGATTGTCCCGAGGTC	CACCGGTGTCTAGGAAAATGATGG

Immunostaining and Quantification—For antigen retrieval, paraffin-embedded sections were submerged in citrate buffer and heated in a microwave pressure cooker (pH 6 for 15 minutes). Sections were blocked in 10% (v/v) normal goat serum for 1 hour at room temperature. Primary antibodies were diluted in 10% (v/v) normal goat serum and incubated at 4°C in a humidified chamber (refer to Key Resources Table). Biotinylated secondary antibodies from the Avidin Biotin Complex ABC-kit (Vector Laboratories) was used according to the manufacturer's instructions. Antigen visualisation was achieved using 3,3-Diaminobenzine (DAB, DAKO). Images were collected and analyzed with Aperio ImageScope v11.2.0.780 software. Quantification of positive staining per mm^2 was performed using an automated cell counter script in FIJI (ImageJ).

Immunofluorescence—Automated staining was performed using the DAKO Omnis system according to the manufacturer's protocol. For antigen retrieval, paraffin-embedded sections were heated in Envision Flex Target Retrieval Solution. Primary antibodies were diluted in Envision Flex Target Retrieval Solution and incubated at 32°C for 1 hour (refer to Key Resources Table). Fluorescent secondary antibodies purchased from Invitrogen were incubated for 30 minutes. Slides were mounted with ProLong® Gold Antifade Mountant containing DAPI as a nuclei counterstain. Images were collected using the Zeiss Axio Observer microscope.

Isolation and Stimulation of BMDMs—Bone marrow was harvested from the femur and tibia of mice by flushing with sterile PBS. Cells were washed twice in PBS and filtered through a 100mm sieve. The single cell suspension was then cultured in DMEM containing 10% (v/v) FCS and L929 conditioned media. To fully differentiate BMDMs, cells were cultured for 7 days with fresh media changed every other day. Adherent macrophages were detached from plates using a cell-scraper, and cell viability was assessed by trypan blue exclusion. BMDMs were seeded onto 6 well plates at a density of 1×10^6 live cells per well in fresh L929 conditioned media. Where indicated, BMDMs were either unstimulated or stimulated the next day with recombinant mouse IL-4 (20ng/mL, Peprotech), IL-13(20ng/mL, Peprotech), IL-6 (20ng/mL, Peprotech), IL-11 (20ng/mL, Peprotech) or Stattic (10mM, Cayman Chemical) in fresh L929 conditioned media. After 24 hours, wells were washed with ice-cold PBS and adherent macrophages were detached from plates using a cell-scraper.

Isolation of Epithelial and Immune Cells—Epithelial and immune cells were isolated as previously described (Rankin et al., 2016). In brief, tissues were cut into 2mm pieces and

incubated at 37°C in Ca^{2+}- and Mg^{2+}-free Hanks medium plus 1mM EDTA with gentle shaking. After 30 minutes, tissues were vortexed for 30 seconds and the supernatant containing intraepithelial lymphocytes was separated from the tissue fragments and kept on ice. These tissues were further digested in Collagenase/Dispase (Roche) and DNase I (Roche) in Ca^{2+}- and Mg^{2+}-free Hanks medium plus 5% FCS for 45 minutes at 37°C under continuous rotation. Subsequently, samples were vortexed for 30 seconds to dissociate lamina propria leukocytes from the remaining mucosa, and the cell suspensions from both incubations were pooled, filtered and washed in PBS plus 5% FCS for analysis by flow cytometry.

Flow Cytometry—Cells were incubated with fluorophore-conjugated primary antibodies (1:200) for 20 minutes on ice in the dark, washed twice and re-suspended in PBS supplemented with 5% FCS as previously described (Rankin et al., 2016). Flow cytometry was performed on the Fortessa x20 (BD Biosciences) or Aria L cell sorter. Background fluorescence was estimated by substituting the primary antibodies with their specific isotype controls and fluorescent-minus-one controls, as well as using compensation beads and unstained controls (referto Key Resources Table). Dead cells were identified by Propidium iodide staining and excluded from analysis. Analysis of all experiments was performed using compensated data with FlowJo software (Version 10).

RNA-Seq Analysis—In total 622 human colon (COAD) and rectal (READ) tumor RNASEQ gene expression data were retrieved from TCGA data portal (https://tcga-data.nci.nih.gov/tcga/). Expressed genes were filtered by a $\log_2$ read count per million of four in at least 10 tumor samples and further filtered for variable genes with an interquartile range of greater than 0.5. Tumor samples were normalized using TMM (Robinson and Oshlack, 2010) and split into *HCK* high and low expressers based on median gene expression value. Differential genes were identified using the Voom algorithm within LIMMA (Law et al., 2014) and EdgeR (Robinson et al., 2010), FDR adjusted and were considered significantly differential if the adjusted p value was < 0.05 and showed > 2-fold change in expression. Differential genes were separated into upregulated and downregulated gene sets and analysed for significant pathway enrichment against the KEGG PATHWAY database (Kanehisa et al., 2016) with adjusted p value < 0.05 using GOseq (Young et al., 2010).

QUANTIFICATION AND STATISTICAL ANALYSIS

All experiments were performed at least twice with a minimum of three age- and sex-matched mice per group. The specific n (number of animals) used per cohort is indicated in the respective figure legends. For RK20449 studies, mice with comparable tumor sizes were randomized into treatment groups. Tumor growth was measured and recorded by an independent assessor who was blinded to the experimental conditions.

Comparisons between mean values were performed with a 2-tailed Student's *t*-test as appropriate using Prism 6 software (GraphPad). A p value of less than 0.05 was considered statistically significant.

Supplementary Material

Refer to Web version on PubMed Central for supplementary material.

Acknowledgments

We thank the WEHI Flow Cytometry, Animal Facility and Histology Department for excellent technical assistance. This work was made possible through Victorian State Government Operational Infrastructure Support, the Australian Cancer Research Foundation, the National Health and Medical Research Council (NHMRC) of Australia project grants 1008614, 1016647, and 1025239, the Victorian Cancer Agency grant ECSG13041, and the RFA-UD from La Trobe University. M.E. also received funding from Ludwig Cancer Research. A.R.P. is supported by an Australian Post-Graduate Award PhD Scholarship and Cancer Therapeutics CTx PhD Top-Up scholarship. M.E. and O.S. are Research Fellows of the NHMRC.

References

Andreu P, Johansson M, Affara NI, Pucci F, Tan T, Junankar S, Korets L, Lam J, Tawfik D, DeNardo DG, et al. FcRgamma activation regulates inflammation-associated squamous carcinogenesis. Cancer Cell. 2010; 17:121–134. [PubMed: 20138013]

Bailey C, Negus R, Morris A, Ziprin P, Goldin R, Allavena P, Peck D, Darzi A. Chemokine expression is associated with the accumulation of tumour associated macrophages (TAMs) and progression in human colorectal cancer. Clin Exp Metastasis. 2007; 24:121–130. [PubMed: 17390111]

Balakrishnan K, Peluso M, Fu M, Rosin N, Burger J, Wierda W, Keating M, Faia K, O'Brien S, Kutok J, et al. The phosphoinositide-3-kinase (PI3K)-delta and gamma inhibitor, IPI-145 (Duvelisib), overcomes signals from the PI3K/AKT/S6 pathway and promotes apoptosis in CLL. Leukaemia. 2015; 9:1811–1822.

Becker C, Fantini MC, Schramm C, Lehr HA, Wirtz S, Nikolaev A, Burg J, Strand S, Kiesslich R, Huber S, et al. TGF-β suppresses tumor progression in colon cancer by inhibition of IL-6 trans-signaling. Immunity. 2004; 21:491–501. [PubMed: 15485627]

Bhattacharjee A, Pal S, Feldman GM, Cathcart MK. Hck is a key regulator of gene expression in alternatively activated human monocytes. J Biol Chem. 2011; 286:36708–36723.

Biswas SK, Mantovani A. Macrophage plasticity and interaction with lymphocyte subsets: cancer as a paradigm. Nat Immunol. 2010; 11:889–896. [PubMed: 20856220]

Bollrath J, Phesse T, Burstin VV, Putoczki T, Bennecke M, Bateman T, Nebelsiek K, Lundgren-May T, Canli O, Schwitalla S. gp130-mediated Stat3 activation in enterocytes regulates cell survival and cell-cycle progression during colitis-associated tumourigenesis. Cell. 2009; 15:91–102.

Calderwood D, Johnston D, Munschauer R, Rafferty P. Pyrrolo [2,3-d]pyrimidines containing diverse N-7 substituents as potent inhibitors of Lck. Bioorg Med Chem Lett. 2002; 12:1683–1686. [PubMed: 12039590]

Craven B, Zaric V, Martin A, Mureau C, Egan L. Effect of genetic deletion or pharmacological antagonism of tumor necrosis factor alpha on colitis-associated carcinogenesis in mice. Inflamm Bowel Dis. 2015; 21:485–495. [PubMed: 25581824]

Crowley MT, Costello PS, Fitzer-Attas CJ, Turner M, Meng F, Lowell C, Tybulewicz V, DeFranco A. A critical role for Syk in signal transduction and phagocytosis mediated by Fcγ receptors on macrophages. J Exp Med. 1997; 186:1027–1039. [PubMed: 9314552]

Dai XM, Ryan GR, Hapel AJ, Dominguez MG, Russell RG, Kapp S, Sylvestre V, Stanley ER. Targeted disruption of the mouse colony-stimulating factor 1 receptor gene results in osteopetrosis, mononuclear phagocyte deficiency, increased primitive progenitor cell frequencies, and reproductive defects. Blood. 2002; 99:111–120. [PubMed: 11756160]

DeNardo D, Barreto J, Andreu P, Vasquez L, Tawfik D, Kolhatkar N, Coussens L. CD4(+) T cells regulate pulmonary metastasis of mammary carcinomas by enhancing protumor properties of macrophages. Cancer Cell. 2009; 16:91–102. [PubMed: 19647220]

DeNardo DG, Andreu P, Coussens LM. Interactions between lymphocytes and myeloid cells regulate pro- versus anti-tumor immunity. Cancer Metastasis Rev. 2010; 29:309–316. [PubMed: 20405169]

Edin S, Wikberg M, Dahlin A, Rutegard J, Oberg A, Oldenborg P, Palmqvist P. The distribution of macrophages with a M1 or M2 pheno-type in relation to prognosis and the molecular characteristics of colorectal cancer. PLoS One. 2012; 7:e47045. [PubMed: 23077543]

Ernst M, Gearing D, Dunn A. Functional and biochemical association of Hck with the LIF/IL-6 receptor signal transducing subunit gp130 in embryonic stem cells. EMBO J. 1994; 13:1574–1584. [PubMed: 8156996]

Ernst M, Inglese M, Scholz GM, Harder KW, Clay FJ, Bozinovski S, Waring P, Darwiche R, Kay T, Sly P, et al. Constitutive activation of the Src family kinase Hck results in spontaneous pulmonary inflammatory and an enhanced innate immune response. J Exp Med. 2002; 196:589–604. [PubMed: 12208875]

Germano G, Frapolli R, Belgiovine C, Anselmo A, Pesce S, Liguori M, Erba E, Uboldi S, Zucchetti M, Pasqualini F, et al. Role of macrophage targeting in the antitumor activity of trabectedin. Cancer Cell. 2013; 23:249–262. [PubMed: 23410977]

Gocheva V, Wang HW, Gadea BB, Shree T, Hunter KE, Garfall AL, Berman T, Joyce JA. IL-4 induces cathepsin protease activity in tumor-associated macrophages to promote cancer growth and invasion. Genes Dev. 2010; 24:241–255. [PubMed: 20080943]

Goldman A, Majumder B, Dhawan A, Ravi S, Goldman D, Kohandel M, Majumder PK, Sengupta S. Temporally sequenced anticancer drugs overcome adaptive resistance by targeting a vulnerable chemotherapy-induced phenotypic transition. Nat Commun. 2015; 6:1–13.

Goswami CP, Nakshatri H. PROGgene: gene expression based survival analysis web application for multiple cancers. J Clin Bioinforma. 2013; 3:22. [PubMed: 24165311]

Guryanova OA, Wu Q, Cheng L, Lathia JD, Huang Z, Yang J, MacSwords J, Eyler CE, McLendon RE, Heddleston JM, et al. Nonreceptor tyrosine kinase BMX maintains self-renewal and tumorigenic potential of glioblastoma stem cells by activating STAT3. Cancer Cell. 2011; 19:498–511. [PubMed: 21481791]

Hibbs M, Tarlinton D, Armes J, Grail D, Hodgson G, Maglitto R, Stacker S, Dunn A. Multiple defects in the immune system of Lyn-deficient mice, culminating in autoimmune disease. Cell. 1995; 83:301–311. [PubMed: 7585947]

Irby R, Mao W, Coppola D, Kang J, Loubeau J, Trudeau W, Karl R, Fujita D, Jove R, Yeatman T. Activating SRC mutation in a subset of advanced human colon cancers. Nat Genet. 1999; 21:187–190. [PubMed: 9988270]

Isella C, Terrasi A, Bellomo S, Petti C, Galatola G, Muratore A, Mellano A, Senetta R, Cassenti A, Sonetto C, et al. Stromal contribution to the colorectal cancer transcriptome. Nat Genet. 2015; 47:312–319. [PubMed: 25706627]

Ji H, Rintelen F, Waltzinger C, Meier DB, Bilancio A, Pearce W, Hirsch E, Wymann MP, Rückle T, Camps M, et al. Inactivation of PI3Kγ and PI3Kδ distorts T-cell development and causes multiple organ inflammation. Blood. 2007; 110:2940–2947. [PubMed: 17626838]

Kadl A, Meher A, Sharma P, Lee MY, Doran AC, Johnstone SR, Elliott MR, Gruber F, Han J, Chen W, et al. Identification of a novel macrophage phenotype that develops in response to atherogenic phospholipids via Nrf2. Circ Res. 2010; 107:737–746. [PubMed: 20651288]

Kanehisa M, Sato Y, Kawashima M, Furumichi M, Tanabe M. KEGG as a reference resource for gene and protein annotation. Nucleic Acids Res. 2016; 44:D457–D462. [PubMed: 26476454]

Kieckbusch J, Balmas E, Hawkes D, Colucci F. Disrupted PI3K p110δ signaling dysregulates maternal immune cells and increases fetal mortality in mice. Cell Rep. 2015; 12:2817–2828.

Kovács M, Németh T, Jakus Z, Sitaru C, Simon E, Futosi K, Botz B, Helyes Z, Lowell CA, Mócsai A. The Src family kinases Hck, Fgr, and Lyn are critical for the generationof thein vivo inflammatory environment without a direct role in leukocyte recruitment. J Exp Med. 2014; 211:1993–2011. [PubMed: 25225462]

Kubo T, Kuroda Y, Shimizu H, Kokubu A, Okada N, Hosoda F, Arai Y, Nakamura Y, Taniguchi H, Yanagihara K, et al. Resequencing and copy number analysis of the human tyrosine kinase gene family inpoorly differentiated gastric cancer. Carcinogenesis. 2009; 30:1857–1864. [PubMed: 19734198]

Kuperman D, Schofield B, Wills-Karp M, Grusby M. Signal transducer and activator of transcription factor 6 (Stat6)-deficient mice are protected from antigen-induced airway hyperresponsiveness and mucus production. J Exp Med. 1998; 187:939–948. [PubMed: 9500796]

Lacey D, Achuthan A, Fleetwood A, Dinh H, Roiniotis J, Scholz G, Chang M, Beckman S, Cook A, Hamilton J. Defining GM-CSF- and macrophage-CSF-dependent macrophage responses by in vitro models. J Immunol. 2012; 188:5752–5765. [PubMed: 22547697]

Lang R, Patel D, Morris J, Rutschman R, Murray P. Shaping gene expression in activated and resting primary macrophages by IL-10. J Immunol. 2002; 169:2253–2263. [PubMed: 12193690]

Lanskron G, De la Fuente M, Thuwajit P, Thuwajit C, Hermoso M. Chronic inflammation and cytokines in the tumour microenvironment. J Immunol Res. 2014; 2014:1–19.

Law CW, Chen Y, Shi W, Smyth GK. voom: precision weights unlock linear model analysis tools for RNA-seq read counts. Genome Biol. 2014; 15:R29. [PubMed: 24485249]

Lowell C, Benton G. Resistance to endotoxic shock and reduced neutrophil migration in mice deficient for the Src-family kinases Hck and Fgr. Proc Natl Acad Sci USA. 1998; 95:7580–7584. [PubMed: 9636192]

Lowell CA, Soriano P, Varmus HE. Functional overlap in the src gene family: inactivation of hck and fgr impairs natural immunity. Genes Dev. 1994; 8:387–398. [PubMed: 8125254]

Mantovani A. Macrophages, neutrophils, and cancer: a double edged sword. N J Sci. 2014; 214:1–14.

Marino M, Dunn A, Grail D, Inglese M, Noguchi Y, Richards E, Jungbluth A, Wada H, Moore M, Williamson B, et al. Characterization of tumor necrosis factor-deficient mice. Proc Natl Acad Sci USA. 1997; 94:8093–8098. [PubMed: 9223320]

Mazzi P, Caveggion E, Lapinet-Vera J, Lowell C, Berton G. The Src-family kinases Hck and Fgr regulateearly lipopolysaccharide-induced myeloid cell recruitment into the lung and their ability to secrete chemokines. J Immunol. 2015; 195:2383–2395. [PubMed: 26232427]

Medina I, Cougoule C, Drechsler M, Bermudez B, Koenen RR, Sluimer J, Wolfs I, Do¨ ring Y, Herias V, Gijbels M, et al. Hck/Fgr kinase deficiency reduces plaque growth and stability by blunting monocyte recruitment and intraplaque motility. Circulation. 2015; 132:490–501. [PubMed: 26068045]

Miller, L. 2010. http://lukemiller.org/index.php/2010/11/analyzing-gels-and-western-blots-with-image-j/

Mombaerts P, Iacomini J, Johnson R, Herrup K, Tonegawa S, Papaioannou V. RAG-1-deficient mice have no mature B and T lymphocytes. Cell. 1992; 68:869–877. [PubMed: 1547488]

Neufert C, Becker C, Neurath MF. An inducible mouse model of colon carcinogenesis for the analysis of sporadic and inflammation-driven tumor progression. Nat Protoc. 2007; 2:1998–2004. [PubMed: 17703211]

Oshima H, Ishikawa T, Yoshida G, Naoi K, Maeda Y, Naka K, Ju X, Yamada Y, Minamoto T, Mukaida N, et al. TNF-a/TNFR1 signaling promotes gastric tumorigenesis through induction of Noxo1 and Gna14 in tumor cells. Oncogene. 2014; 33:3820–3829. [PubMed: 23975421]

Ostrand-Rosenberg S, Grusby M, Clements V. Cutting edge: STAT6-deficient mice have enhanced tumor immunity to primary and metastatic mammary carcinoma. J Immunol. 2000; 165:6015–6019. [PubMed: 11086031]

Pedroza-Gonzalez A, Xu K, Wu TC, Aspord C, Tindle S, Marches F, Gallegos M, Burton EC, Savino D, Hori T, et al. Thymic stromal lymphopoietin fosters human breast tumor growth by promoting type 2 inflammation. J Exp Med. 2011; 208:479–490. [PubMed: 21339324]

Pello O, Pizzol MD, Mirolo M, Soucek L, Zammataro L, Amabile A, Doni A, Nebuloni M, Swigart L, Evan G, et al. Role of c-MYC in alternative activation of human macrophages and tumor-associated macrophage biology. Blood. 2012; 119:411–421. [PubMed: 22067385]

Pene-Dumitrescu T, Shu S, Wales T, Alvarado J, Shi H, Narute P, Moroco J, Yeh J, Engen J, Smithgall T. HIV-1 Nef interaction influences the ATP-binding site of the Src-family kinase, Hck. BMC Chem Biol. 2012; 12:1–12. [PubMed: 22420777]

Poh AR, O'Donoghue RJJ, Ernst M. Hematopoietic cell kinase (HCK) as a therapeutic target in immune and cancer cells. Oncotarget. 2015; 6:15752–15771. [PubMed: 26087188]

Popivanova B, Kitamura K, Wu Y, Kondo T, Kagaya T, Kaneko S, Oshima M, Fujii C, Mukaida N. Blocking TNF-alpha in mice reduces colorectal carcinogenesis associated with chronic colitis. J Clin Invest. 2008; 118:560–570. [PubMed: 18219394]

Putoczki T, Thiem S, Loving A, Busuttil R, Wilson N, Ziegler P. Interleukin-11 is the dominant IL-6 family cytokine during gastrointestinal tumourigenesis and can be targeted therapeutically. Cancer Cell. 2013; 24:257–271. [PubMed: 23948300]

Pyonteck SM, Akkari L, Schuhmacher AJ, Bowman RL, Sevenich L, Quail DF, Olson OC, Quick ML, Huse JT, Teijeiro V, et al. CSF-1R inhibition alters macrophage polarization and blocks glioma progression. Nat Med. 2013; 19:1264–1272. [PubMed: 24056773]

Qian BZ, Pollard JW. Macrophage diversity enhances tumor progression and metastasis. Cell. 2010; 141:39–51. [PubMed: 20371344]

Rankin LC, Girard-Madoux MJH, Cyril Seillet LAM, Kerdiles Y, Fenis A, Wieduwild E, Putoczki T, Mondot S, Lantz O, Demon D, et al. Complementarity and redundancy of IL-22-producing innate lymphoid cells. Nat Immunol. 2016; 17:179–186. [PubMed: 26595889]

Ries CH, Cannarile MA, Hoves S, Benz J, Wartha K, Runza V, Rey-Giraud F, Pradel LP, Feuerhake F, Klaman I, et al. Targeting tumor-associated macrophages with anti-CSF-1R antibody reveals a strategy for cancer therapy. Cancer Cell. 2014; 25:846–859. [PubMed: 24898549]

Robinson MD, Oshlack A. A scaling normalization method for differential expression analysis of RNA-seq data. Genome Biol. 2010; 11:R25. [PubMed: 20196867]

Robinson M, McCarthy D, Smyth G. edgeR: a Bioconductor package for differential expression analysis of digital gene expression data. Bioinformatics. 2010; 26:139–140. [PubMed: 19910308]

Rody A, Holtrich U, Pusztai L, Liedtke C, Gaetje R, Ruckhaeberle E, Solbach C, Hanker L, Ahr A, Metzler D, et al. T-cell metagene predicts a favorable prognosis in estrogen receptor-negative and HER2-positive breast cancers. Breast Cancer Res. 2009; 11:1–15.

Ruffell B, Chang-Strachan D, Chan V, Rosenbusch A, Ho CMT, Pryer N, Daniel D, Hwang S, Rugo HS, Coussens LM. Macrophage IL-10 blocks CD8+ T cell-dependent responses to chemotherapy by suppressing IL-12 expression in intratumoral dendritic cells. Cancer Cell. 2014; 26:623–637. [PubMed: 25446896]

Saito Y, Yuki H, Kuratani M, Hashizume Y, Takagi S, Honma T, Tanaka A, Shirouzu M, Mikuni J, Handa N, et al. A pyrrolo-pyrimidine derivative targets human primary AML stem cells in vivo. Sci Transl Med. 2013; 5:181ra152.

Schaeffer M, Schneiderbauer M, Weidler S, Tavares R, Warmuth M, Vos GD, Hallek M. Signaling through a novel domain of gp130 mediates cell proliferation and activation of Hck and Erk kinases. Mol Cell Biol. 2001; 21:8068–8081. [PubMed: 11689697]

Schindler T, Sicheri F, Pico A, Gazit A, Levitzki A, Kuriyan J. Crystal structure of Hck in complex with a Src family-selective tyrosine kinase inhibitor. Mol Cell. 1999; 3:639–648. [PubMed: 10360180]

Snyder M, Bishop J. A mutation at the major phosphotyrosine in pp60v-src alters oncogenic potential. Virology. 1984; 136:375–386. [PubMed: 6205504]

Stamm L, Raisanen-Sokolowski A, Okano M, Russell M, David J, Satoskar A. Mice with STAT6-targeted gene disruption develop a Th1 response and control cutaneous leishmaniasis. J Immunol. 1998; 161:6180–6188. [PubMed: 9834104]

Stein P, Vogel H, Soriano P. Combined deficiencies of Src, Fyn, and Yes tyrosine kinases in mutant mice. Genes Dev. 1994; 8:1999–2007. [PubMed: 7958873]

Stritesky G, Muthukrishnan R, Sehra S, Goswami R, Pham D, Travers J, Nguyen E, Levy D, Kaplan M. The transcription factor STAT3 is required for T helper 2 cell development. Immunity. 2011; 34:39–49. [PubMed: 21215659]

Takeda K, Tanaka T, Shi W, Matsumoto M, Minami M, Kashiwamura S, Nakanishi K, Yoshida N, Kishimoto T, Akira S. Essential role of Stat6 in IL-4 signalling. Nature. 1996; 380:627–630. [PubMed: 8602263]

Terabe M, Matsui S, Park J, Mamura M, Noben-Trauth N, Donaldson D, Chen W, Wahl S, Ledbetter S, Pratt B, et al. Transforming growth factor-beta production and myeloid cells are an effector mechanism through which CD1d-restricted T cells block cytotoxicTlymphocyte-mediated tumor

immunosurveillance: abrogation prevents tumor recurrence. J Exp Med. 2003; 198:1741–1752. [PubMed: 14657224]

Thiem S, Pierce TP, Palmieri M, Putoczki TL, Buchert M, Preaudet A, Farid RO, Love C, Catimel B, Lei Z, et al. mTORC1 inhibition restricts inflammation-associated gastrointestinal tumorigenesis in mice. J Clin Invest. 2013; 123:767–780. [PubMed: 23321674]

Wang Q, Ni H, Lan L, Wei X, Xiang R, Wang Y. Fra-1 protooncogene regulates IL-6 expression in macrophages and promotes the generation of M2d macrophages. Cell Res. 2010; 20:701–712. [PubMed: 20386569]

Wick EC, LeBlanc RE, Ortega G, Robinson C, Platz E, Pardoll DM, Iacobuzio-Donahue C, Sears CL. Shift from pStat6 to pStat3 predominance is associated with inflammatory bowel disease-associated dysplasia. Inflamm Bowel Dis. 2012; 18:1267–1274. [PubMed: 22021169]

Yokozeki H, Ghoreishi M, Takagawa S, Takayama K, Satoh T, Katamama I, Takeda K, Akira S, Nishioka N. Signal transducer and activator of transcription 6 is essential in the induction of contact hyper-sensitivity. J Exp Med. 2000; 191:995–1004. [PubMed: 10727461]

Young MD, Wakefield MJ, Smyth GK, Oshlack A. Gene ontology analysis for RNA-seq: accounting for selection bias. Genome Biol. 2010; 11:R14. [PubMed: 20132535]

Ziegler SF, Marth JD, Lewis DB, Perlmutter R. Novel protein-tyrosine kinase gene (hck) preferentially expressed in cells of hematopoietic origin. Mol Cell Biol. 1987; 7:2276–2285. [PubMed: 3453117]

Highlights

- Abundant HCK in tumor leukocytes of human colon cancer correlates with poor survival
- Excessive myeloid HCK activity results in alternative macrophage polarization
- Myeloid HCK promotes colon tumorigenesis associated with increased Stat3 activity
- Ablation of HCK or its therapeutic inhibition limits colon cancer xenograft growth

Significance

Excessive activity of SRC family kinases (SFK) results in the transformation of cells and the associated development of solid and hematological malignancies. Here we provide functional evidence for the capacity of dysregulated SFK activity within the stromatopromote the growth of colon cancerin mice irrespective of coinciding chronic inflammation. Rather than modifying immune cell infiltration of tumors, Hck activity promotes polarization of tumor-associated macrophages toward a tumor-promoting M2-like endotype and the accumulation of IL-6/lL-11 family cytokines, which drive a Stat3-dependent growth response in neoplastic cells. Accordingly, inhibition of Hck activity reduces tumor burden in mice, while low expression of *HCK* in colorectal cancer is associated with prolonged patient survival.

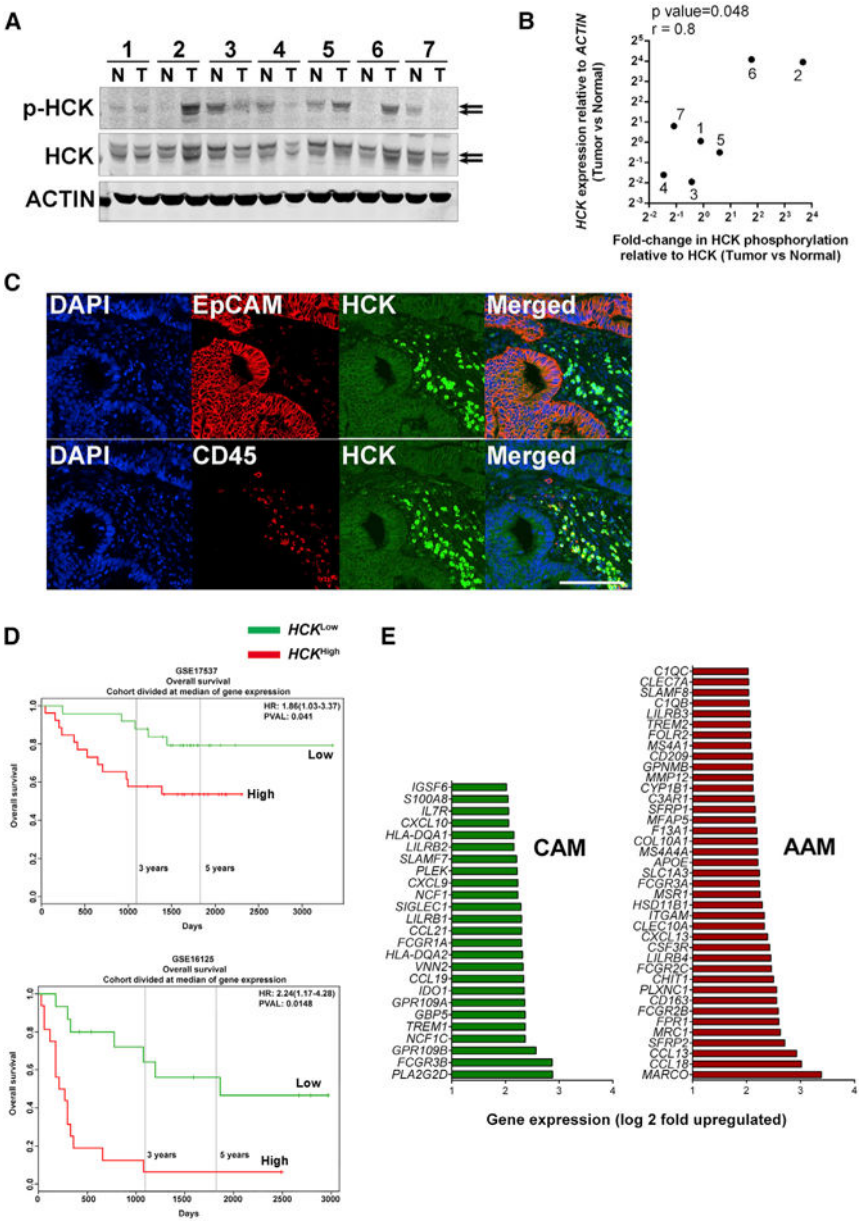

Figure 1. *HCK* Expression Correlates with Poor Survival and Increased Expression of Genes Related to Alternative Activation of Macrophages

(A) Western blot analysis of the phosphorylated protein isoforms of p59/61HCK (arrows) in paired biopsies of normal human colon (N) and corresponding CRC adenocarcinoma (T). To assess for protein abundance, the membrane was probed for ACTIN.

(B) Correlation between *HCK* mRNA expression (fold-change relative to *ACTIN*) and abundance of phosphorylated p-HCK (fold-change relative to total HCK protein) expressed as fold-change in paired biopsies of normal human colon and CRC tumors analyzed in (A). Numbers refer to individual patient samples. Pearson correlation coefficient and p value are indicated.

(C) Immunofluorescence staining of HCK, CD45, and EpCAM in a representative sample from the matched human CRC tumors in (A). Nuclei are visualized by DAPI staining. Scale bar, 100 μm.

(D) Overall survival of human sporadic CRC patients from two independent datasets (GEO: GSE16125 and GSE17537) and assigned at the median of *HCK* expression into HCK^{Low} and HCK^{High} cohorts.

(E) Analysis of genes differentially expressed between HCK^{Low} and HCK^{High} human sporadic colorectal tumors using the TCGA dataset (see Supplemental Information). Of the top 100 overexpressed genes in the HCK^{High} cohort, those associated with CAM or AAM polarization are shown (see text).

See also Figure S1 and Table S1.

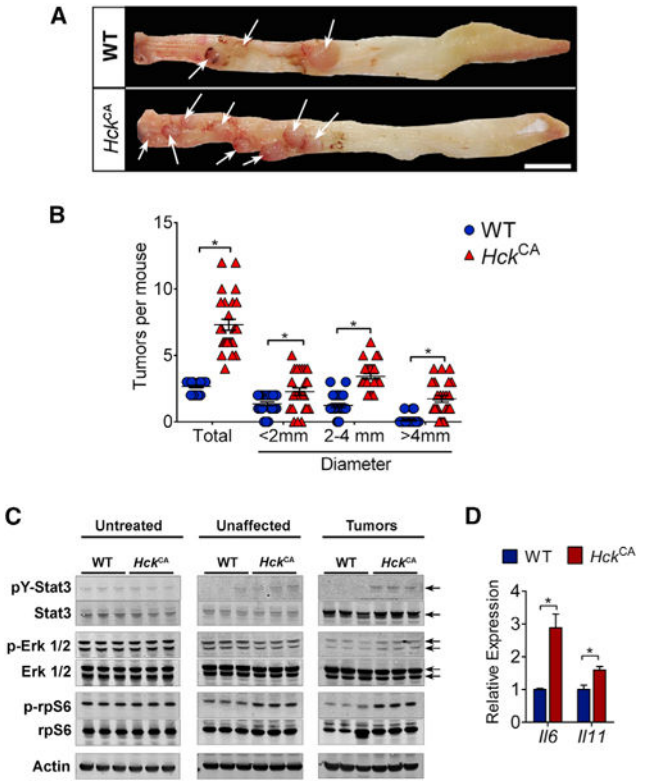

Figure 2. Constitutive Hck Activation Enhances Sporadic Colorectal Tumor Development in Mice

(A) Photomicrograph of representative colons from WT and *Hck*^{CA} mice collected 16 weeks after the last of 6 consecutive challenges with AOM to induce sporadic CRC. Arrows indicate tumors. Scale bar, 1 cm.

(B) Enumeration of total tumor burden and of tumors following classification according to their size. Each symbol represents data from an individual mouse treated as described for (A). *$p < 0.001$.

(C) Western blot analysis of tumor cell lysates from individual mice treated as described for (A). The Stat3 and Erk1/2 isoforms are indicated by arrows. Membranes were probed sequentially using actin and Erk1/2 as loading controls.

(D) *Il6* and *Il11* mRNA expression in tumors of WT and *Hck*^{CA} mice, n = 3 mice per cohort. *$p < 0.05$.

All data are represented as mean ± SEM, with p values from unpaired Student's t test.

See also Figure S2.

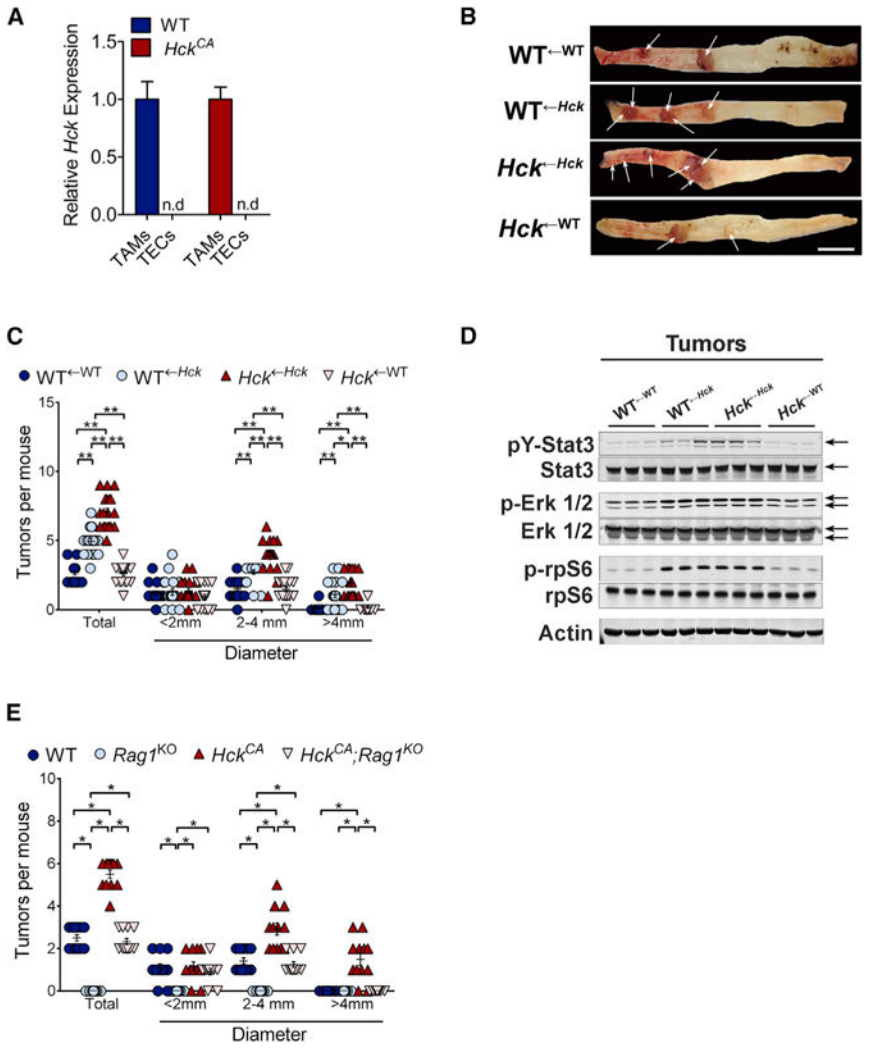

Figure 3. *Hck*^{CA} in Hematopoietic Cells Promotes Sporadic Tumorigenesis

(A) *Hck* mRNA expression of FACS-purified CD45^{+}CD11b^{+}F4/80^{+} tumor-associated macrophages (TAMs) and of EpCAM^{+} tumor epithelial cells (TECs) prepared from tumors of WT and *Hck*^{CA} mice, n = 3 mice per cohort. n.d, not detected.

(B) Photomicrographs of representative colons of reciprocal WT and *Hck*^{CA} bone marrow chimeras collected 16 weeks after the last of 6 consecutive AOM challenges. Arrows indicate tumors. Scale bar, 1 cm.

(C) Enumeration of total tumor burden and of tumors following classification according to their size. Each symbol represents data from an individual mouse as described for (B). *p < 0.01, **p < 0.001.

(D) Western blot analysis of tumor cell lysates from individual mice as described for (B). The Stat3 and Erk1/2 isoforms are indicated by arrows. Actin was used as a loading control for the blot showing the phosphorylated isoforms; Erk1/2 was used as the loading control for blots showing the un-phosphorylated isoforms.

(E) Enumeration of total tumor burden and of tumors following classification according to their size. Each symbol represents data from an individual mouse collected 16 weeks after the last of 6 consecutive challenges with AOM to induce sporadic CRC. **$p < 0.001$. All data are represented as mean ± SEM, with p values from unpaired Student's t test, See also Figure S3.

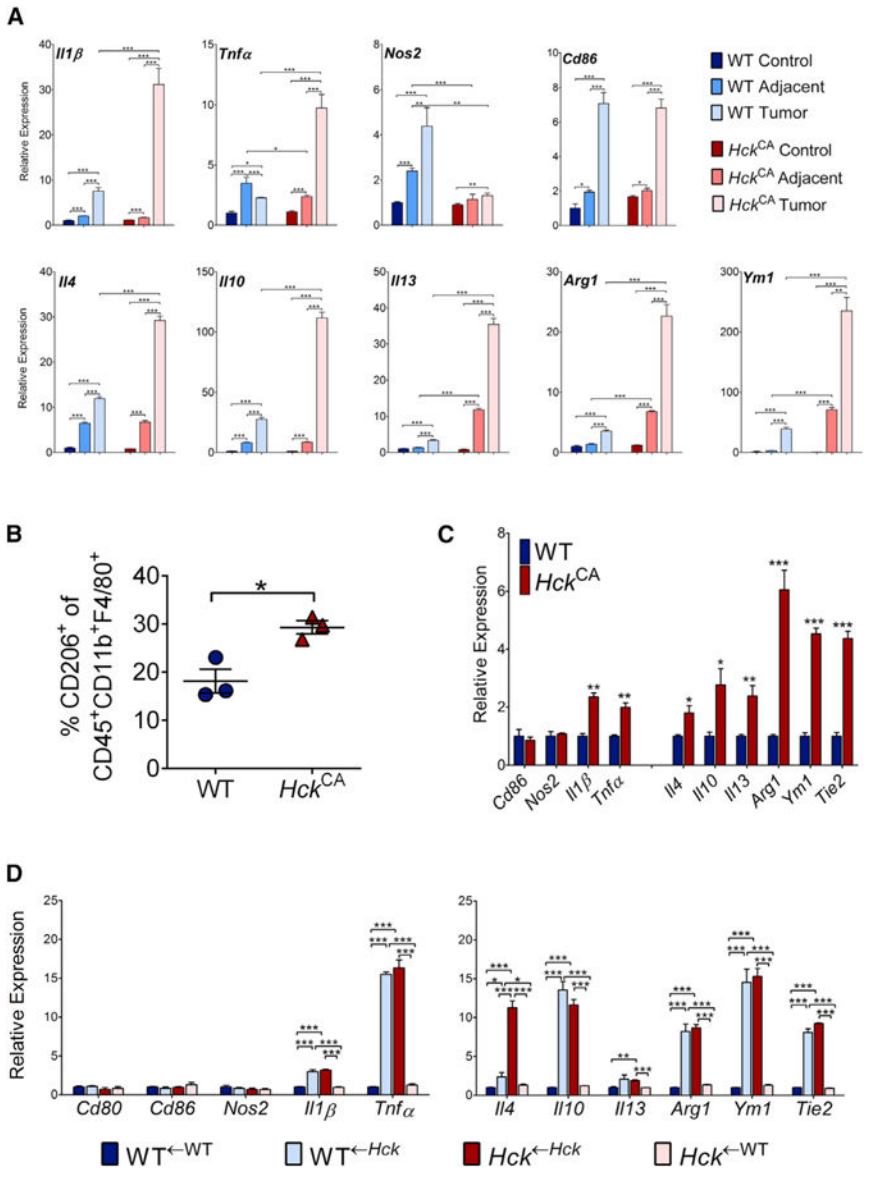

Figure 4. Enhanced Hck Activation in Sporadic Colon Tumors Correlates with an Alternatively Activated Macrophage Gene Signature

(A) qPCR analysis for the expression of genes associated with CAM (*Il1β, Tnfα., Nos2*, and *CD86*) and AAM activation (*Il4, Il10, Il13, Arg1*, and *Ym1*) in tumors and adjacent unaffected colon sections of WT and *Hck*^{CA} mice, either treatment-naive (control) or 16 weeks after the last of 6 consecutive challenges with AOM to induce sporadic CRC, n ≥ 4 mice per cohort.

(B) Quantification of CD206^{+} macrophages (CD45^{+}CD11b^{+}F4/80^{+}) by flow cytometry from sporadic colon tumors of WT and *Hck*^{CA} mice 16 weeks after the last of 6 consecutive AOM challenges. Each symbol represents data from an individual mouse.

(C) qPCR analysis on FACS-purified CD45^{+} CD11b^{+}F4/80^{+} tumor-associated macrophages for CAM- (*Cd86, Nos2, Il1β*, and *Tnfα*) and AAM-associated genes (*Il4, Il10, Il13, Arg1, Ym1*, and *Tie2*), n = 3 mice per cohort.

(D) qPCR analysis on FACS-purified $CD45^+$ $CD11b^+F4/80^+$ tumor-associated macrophages collected from reciprocal bone marrow chimeras of the indicated genotypes, n = 4 mice per cohort. All data are represented as mean ± SEM, with p values from unpaired Student's t test, *p < 0.05, **p < 0.01, ***p < 0.001.

See also Figure S4.

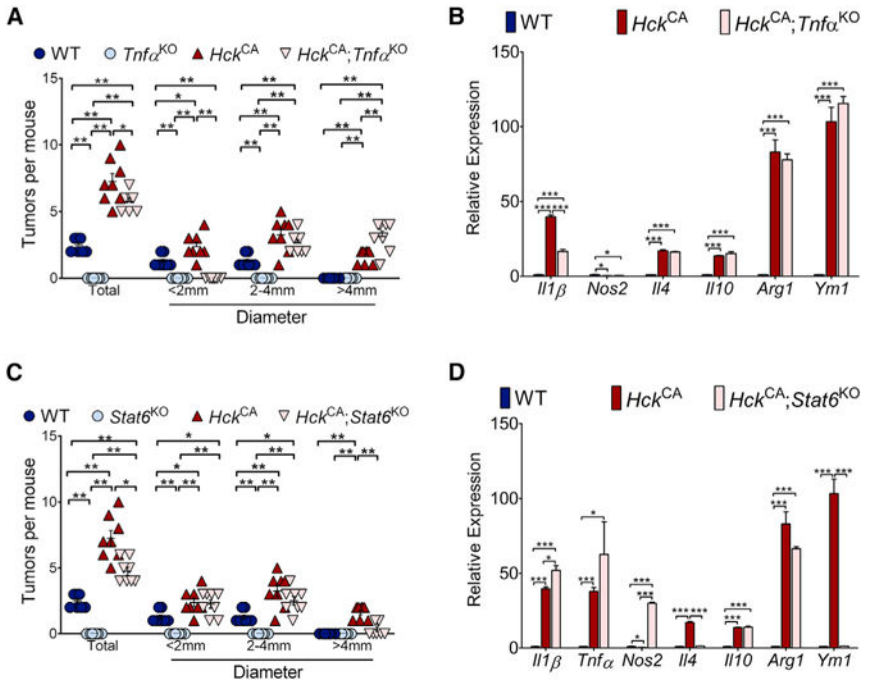

Figure 5. Enhanced Hck Activation Drives Sporadic Colon Tumorigenesis and AAM Differentiation through Non-canonical Pathways

(A and C) Enumeration of total tumor burden and of tumors following classification according to their size. Each symbol represents data from an individual mouse collected 16 weeks after the last of 6 consecutive challenges with AOM to induce sporadic CRC. *p < 0.01, **p < 0.001.

(B and D) qPCR expression analysis of CAM- (*Il1β, Tnfα*, and *Nos2*) and AAM-associated genes (*Il4, Il10, Arg1*, and *Ym1*) in tumors of mice of the indicated genotype, n ≥ 4 mice per cohort. *p < 0.05, **p < 0.01, ***p < 0.001.

All data are represented as mean ± SEM, with p values from unpaired Student's t test.

See also Figure S5.

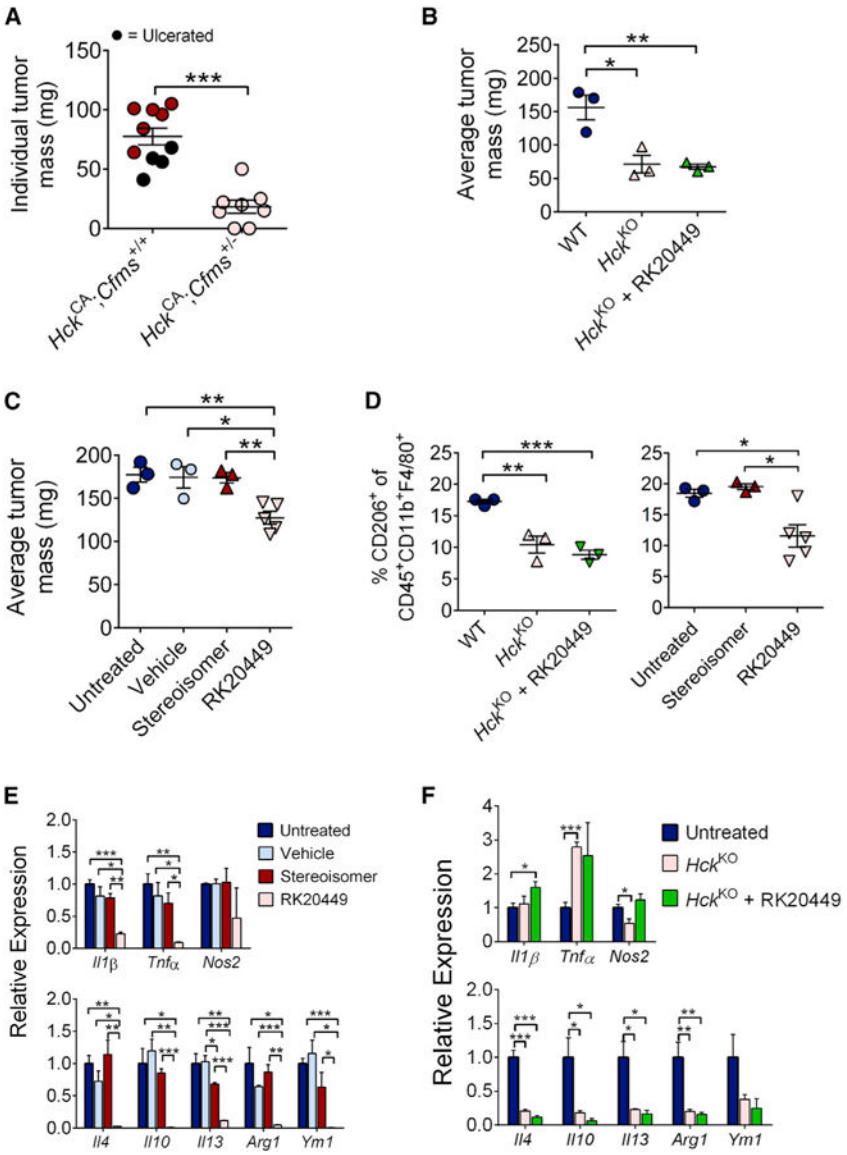

Figure 6. Genetic or Pharmacologic Inhibition of Hck Signaling Restrains Growth of MC38 CRC Allografts

(A) Weight of individual subcutaneous tumors from *Hck*^{CA};*Cfms*$^{+/+}$ or *Hck*^{CA};*Cfms*$^{+/-}$ hosts following inoculation of syngeneic MC38 cells. Each symbol represents a tumor from an individual mouse. Some tumors required earlier collection due to excessive ulceration.

(B) Weight of allograft tumors excised from WT or *Hck*^{KO} mice. Where indicated, mice were treated for 1 week with RK20449 (30 mg/kg) when allografts became palpable. Each symbol represents data from an individual mouse.

(C) Weight of allograft tumors excised from WT mice after systemic treatment with vehicle (12% Captisol), inactive stereoisomer (30 mg/kg), or RK20449 (30 mg/kg) for 1 week. Treatment commenced when allografts became palpable. Each symbol represents data from an individual mouse.

(D) Flow cytometric quantification of CD206-expressing $CD45^+CD11b^+F4/80^+$ macrophages isolated from allografts grown in mice treated as in (B) and (C). Each symbol represents data from an individual mouse.

(E) qPCR analysis on whole-allograft tumors of the indicated treatment cohort from (C), n = 3 mice per cohort.

(F) qPCR analysisonwhole-allograft tumors grown in the mice of the indicated genotypes and treated as in (B), n = 3 mice per cohort.

All data are represented as mean ± SEM, with p values from unpaired Student's t test. *p < 0.05, **p < 0.01, ***p < 0.001.

See also Figure S6.

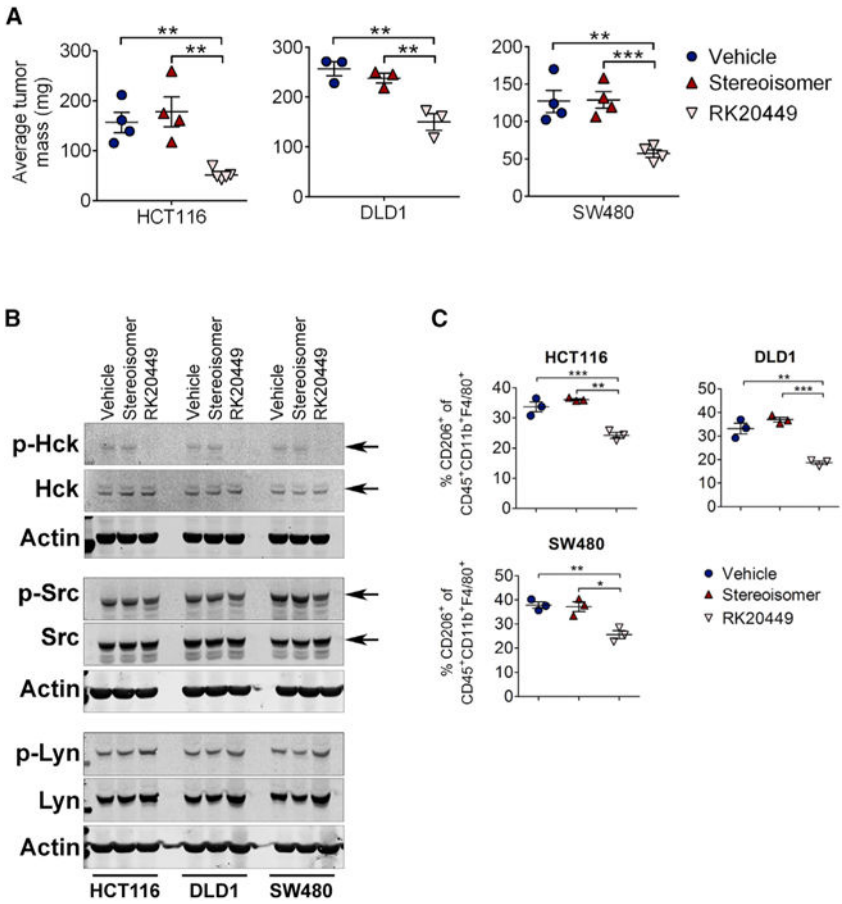

Figure 7. Pharmacologic Inhibition of Hck Signaling Impairs Growth of Human CRC Xenografts

(A) Weight of xenograft tumors excised from *Rag1*^{KO} mice treated with RK20449 (30 mg/kg), its biologically inactive stereoisomer (30 mg/kg), or vehicle. Mice were treated for 10 days once subcutaneous xenografts became palpable. Each symbol represents data from an individual mouse.

(B) Western blot analysis for the phosphorylated forms of selected SFKs in HCT116, DLD1 and SW480 xenografts excised from mice of the indicated treatment cohort. Each lane represents an individual mouse treated as described in (A). The mouse p56/59Hck and p60Src isoforms are indicated by arrows. Actin was used as a loading control.

(C) Flow cytometric quantification of CD206-expressing $CD45^+CD11b^+F4/80^+$ macrophages isolated from HCT116, DLD1, and SW480 CRC cell xenografts grown in mice treated as in (A). Each symbol represents data from an individual mouse.

All data are represented as mean ± SEM, with p values from unpaired Student's t test. *$p < 0.05$, **$p < 0.01$, ***$p < 0.001$.

See also Figure S7.

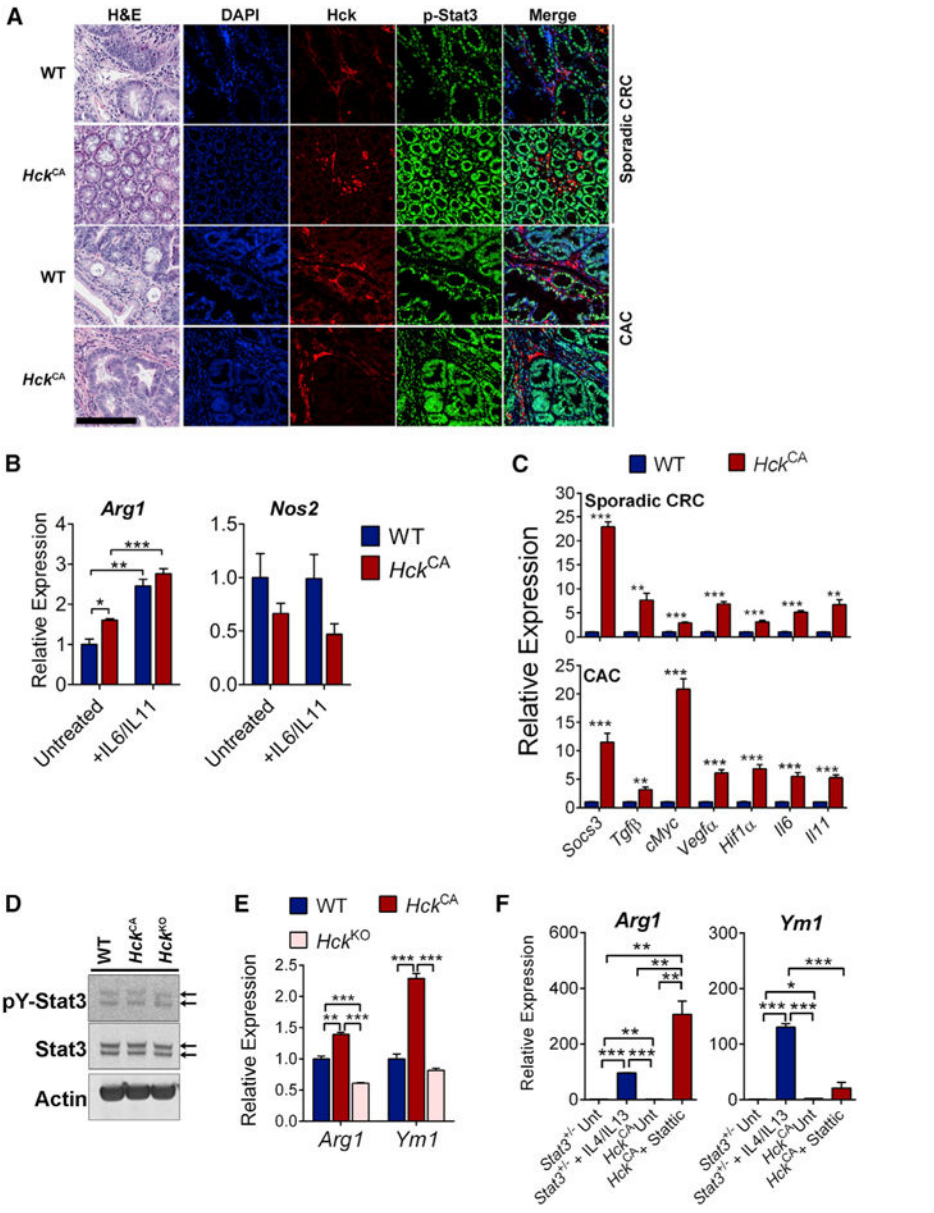

Figure 8. Hck Mediates Induction of the AAM Endotype Independently of Stat3

(A) Representative H&E and co-immunofluorescence stains for Hck and p-Stat3 on WT and *Hck*^{CA} sporadic CRC and CAC tumors. Nuclei are visualized by DAPI staining. Scale bar, 100 μm.

(B) *Arg1* and *Nos2* mRNA expression in naive (untreated) and IL-6/IL-11-stimulated WT and *Hck*^{CA} BMDMs, n = 3 mice per cohort.

(C) qPCR expression analysis for Stat3-target genes on FACS-purified CD45^{+}CD11b^{+}F4/80^{+} macrophages collected from sporadic CRC and CAC tumors of WT and *Hck*^{CA} mice, n = 4 mice per cohort.

(D) Western Blot analysis for phosphorylated Stat3 in naive WT, *Hck*^{CA}, and *Hck*^{KO} BMDMs. The Stat3 isoforms are indicated by arrows. Actin was used as a loading control.

(E) *Arg1* and *Ym1* mRNA expression in naive BMDMs of the indicated genotypes from (D), n = 3 mice per cohort.

(F) *Arg1* and *Ym1* mRNA expression in $Stat3^{+/-}$ and Hck^{CA} BMDMs either treated with IL-4/IL-13 (20 ng/mL) or Stattic (10 μM), n = 3 mice per cohort. Data are represented as mean ± SEM, with p values from unpaired Student's t test, *p < 0.05, **p < 0.01, ***p < 0.001.

See also Figure S8.